DETERMINATION OF HEAT (MASS) TRANSFER FROM BLOCKAGES WITH ROUND AND ELONGATED HOLES IN A WIDE RECTANGULAR CHANNEL

A Thesis

by

VENKATA PANDURANGA PRAVEEN RUPAKULA

Submitted to the Office of Graduate Studies of
Texas A&M University
in partial fulfillment of the requirements for the degree of

MASTER OF SCIENCE

December 2005

Major Subject: Mechanical Engineering

DETERMINATION OF HEAT (MASS) TRANSFER FROM BLOCKAGES WITH ROUND AND ELONGATED HOLES IN A WIDE RECTANGULAR CHANNEL

A Thesis

by

VENKATA PANDURANGA PRAVEEN RUPAKULA

Submitted to the Office of Graduate Studies of
Texas A&M University
in partial fulfillment of the requirements for the degree of

MASTER OF SCIENCE

Approved by:

Co-Chairs of Committee,	Sai C Lau
	Debjyoti Banerjee
Committee Members,	Hamn Ching Chen
	Je Chin Han
Department Head,	Dennis O'Neal

December 2005

Major Subject: Mechanical Engineering

ABSTRACT

Determination of Heat (Mass) Transfer from Blockages with Round and Elongated Holes in a Wide Rectangular Channel. (December 2005)

Venkata Panduranga Praveen Rupakula, B.S.,

Jawaharlal Nehru Technological University, India.

Co-Chairs of Advisory Committee: Dr. Sai C. Lau and Dr. Debjyoti Banerjee

Mass transfer experiments were conducted to study the thermal performance characteristics of blockages with round and elongated holes, positioned in a 12:1 rectangular channel. Naphthalene sublimation technique was adopted to conduct experiments with four different blockage configurations, flow rates corresponding to Reynolds numbers (based on channel hydraulic diameter) of 7,000 and 17,000, and at three blockage locations. The hole area to channel area ratio for all four blockage configurations was the same at 0.196. The hole width was half the channel height, and the distance between consecutive blockages was twice the channel height. Average heat transfer, local heat (mass) transfer and overall pressure drop results were obtained. The thermal performance for a particular blockage configuration was measured in terms of the heat transfer enhancement and the friction factor ratio. Heat transfer enhancement was measured as a ratio of average Nusselt number on the blockage surface to the Nusselt number for a thermally fully developed turbulent flow in a smooth channel. Results indicate that this ratio ranged between 3.6 and 12.4, while the friction factor ratio varied between 500-1700. The blockage configuration with round holes was found to yield best thermal performance, while the configuration with largest hole elongation was nearly equal in thermal performance. In order to compare different blockage configurations, an average value of upstream and downstream side thermal performances was used.

A general downward trend in Nusselt number ratio with elongation of holes was observed on the upstream side and a reverse trend was observed on the downstream side. An upward trend in the Nusselt number ratio with blockage hole elongation on the downstream side of a blockage was primarily due to jet reversal from the downstream blockage and its impingement on the downstream surface of the upstream blockage. Local experiments were performed to compare against the results from average experiments and also to gain insights into the flow behaviour. There was good agreement between the results from local and average mass transfer experiments. The average variation in Nusselt number ratio between local and average mass transfer experiments was about 5.06%.

DEDICATION

To all of my teachers

ACKNOWLEDGEMENTS

I have been immensely helped in my research pursuits and I consider it my privilege to thank everyone for their support.

My first thanks go to my foremost teachers - my parents.

I thank Dr. Sai Lau profusely for the remarkable guidance and encouragement throughout my research. Dr. Lau's attention to details and his patience have really helped me in achieving more than I thought I could. My sincere thanks to Dr. Debjyoti Banerjee for all the discussions and the interesting questions he had posed that allowed me to think further about the experiments and procedures. I also thank Dr. J.C.Han and Dr. H.C. Chen for their valuable time to serve on my committee.

I express my deep sense of gratitude to Hee Seok Ahn and Sangwon Lee for the time and willingness to share their impeccable knowledge of mass transfer experiments with me. If my advisor and advisory committee members were my inspirational gurus, Sangwon and Hee Seok have been instructional gurus to me.

My whole-hearted thanks go to Mr. Johnny Hallford, Mr. Izzidoro Ramirez and Mr. Mike Walker for their help with CNC manufacturing, support in using instruments, and in machining respectively. I also sincerely appreciate all my friends who have cooperated with me during this intensive research period.

TABLE OF CONTENTS

ABSTRACT……... iii

DEDICATION……... v

ACKNOWLEDGEMENTS……... vi

TABLE OF CONTENTS……... vii

LIST OF FIGURES……... viii

LIST OF TABLES……. xi

NOMENCLATURE…….. xii

CHAPTER

I INTRODUCTION……. 1

II LITERATURE REVIEW…….. 5

III EXPERIMENTAL APPARATUS…… 13

IV BLOCKAGES – DESIGN DETAILS……... 19

V EXPERIMENTAL PROCEDURE…… 24

VI DATA REDUCTION…… 26

VII PRESENTATION AND DISCUSSION OF RESULTS…... 29

Results – Average Heat (Mass) Transfer Experiments…. 29
Results – Local Heat (Mass) Transfer Experiments……. 47

VIII CONCLUSIONS AND RECOMMENDATIONS…… 59

REFERENCES…….. 61

APPENDIX A…… 66

APPENDIX B…… 72

VITA…….. 74

LIST OF FIGURES

FIGURE		Page
1	Internal and external cooling concepts used in modern gas turbines……...	2
2	Schematic of test apparatus for mass transfer and pressure measurement experiments……..	15
3	Front view of the experimental setup……...	16
4	Side view of the experimental setup……	17
5	Instrumentation for measurement of local elevation of naphthalene……...	18
6	Engineering drawing for blockage configuration 1(Third angle projection)...	20
7	Engineering drawing for blockage configuration 2(Third angle projection)...	21
8	Engineering drawing for blockage configuration 3(Third angle projection)...	22
9	Engineering drawing for blockage configuration 4(Third angle projection)…	23
10	Average Nusselt number ratio for different blockage configurations at the first blockage location……..	33
11	Average Nusselt number ratio for different blockage configurations at the second blockage location…….	34
12	Average Nusselt number ratio for different blockage configurations at the third blockage location…….	35
13	Heat transfer coefficient for different blockage configurations at the first blockage location……..	38
14	Heat transfer coefficient for different blockage configurations at the second blockage location……..	39
15	Heat transfer coefficient for different blockage configurations at the third blockage location……..	40

FIGURE Page

16 Thermal performance for different blockage configurations at the first blockage location…….. 42

17 Thermal performance for different blockage configurations at the second blockage location…….. 43

18 Thermal performance for different blockage configurations at the third blockage location…….. 44

19 Friction factor ratio at different blockage locations and for all four blockage configurations……... 46

20 Distribution of Nusselt number ratio, at a Reynolds number of 7,000, on the upstream surface of a round holed blockage (case 1) positioned at the first blockage location in the test channel…… 49

21 Distribution of Nusselt number ratio, at a Reynolds number of 7,000, on the upstream surface of a round holed blockage (case 1) positioned at the second blockage location in the test channel…….. 51

22 Distribution of Nusselt number ratio, at a Reynolds number of 7,000, on the downstream surface of a round holed blockage (case 1) positioned at the second blockage location in the test channel……... 52

23 Distribution of Nusselt number ratio, at a Reynolds number of 17,000, on the upstream surface of a round holed blockage (case 1) positioned at the second blockage location in the test channel……... 53

24 Distribution of Nusselt number ratio, at a Reynolds number of 17,000, on the downstream surface of a round holed blockage (case 1) positioned at the second blockage location in the test channel……... 54

25 Distribution of Nusselt number ratio, at a Reynolds number of 7,000, on the upstream surface of a case 4 blockage (with most elongated holes) positioned at the second blockage location in the test channel…… 56

26 Distribution of Nusselt number ratio, at a Reynolds number of 7,000, on the downstream surface of a case 4 blockage (with most elongated holes) positioned at the second blockage location in the test channel..... 57

FIGURE Page

27 Distribution of Nusselt number ratio, at a Reynolds number of 17,000, on the upstream surface of a case 4 blockage (with most elongated holes) positioned at the second blockage location in the test channel…… 58

28 Distribution of Nusselt number ratio, at a Reynolds number of 17,000, on the downstream surface of a case 4 blockage (with most elongated holes) positioned at the second blockage location in the test channel…… 59

LIST OF TABLES

TABLE		Page
1	Experimental results for case 1 and case 2 blockages at the first blockage location……..	65
2	Experimental results for case 3 and case 4 blockages at the first blockage location……..	66
3	Experimental results for case 1 and case 2 blockages at the second blockage location …….	67
4	Experimental results for case 3 and case 4 blockages at the second blockage location …….	68
5	Experimental results for case 1 and case 4 blockages at the third blockage location …….	69

NOMENCLATURE

D_h	hydraulic diameter of test channel, m
d_p	pipe diameter (internal diameter), m
A_s	surface area of mass convection, m^2
T_o	air temperature at the orifice, K
T_w	temperature at the naphthalene surface, K
P	perimeter of test channel, m
$P_{v,w}$	vapour pressure of naphthalene at the blockage surface, Pa
P_o	upstream pressure at the orifice, Pa
ΔP_o	pressure drop across the orifice, Pa
Δt	effective duration of experiment, s
Δz	local change of elevation on naphthalene surface, m
μ	viscosity of air, Ns/m^2
ρ	density of air, kg/m^3
ρ_s	density of solid naphthalene, kg/m^3
$\overline{\rho}_{v,w}$	vapour density of naphthalene on naphthalene surface, kg/m^3

σ	mass diffusion coefficient of naphthalene vapour in air, m^2s
R	gas constant of air in J/Kg K
R_n	gas constant of naphthalene in J/Kg K
$\dot{m}$	mass flow rate of air, Kg/s
ΔM_n	mass of naphthalene convected during the experiment, Kg
Δp	pressure drop across any blockage, Pa
Pr	Prandtl number for air
Sc	Schmidt number for air
$\dot{V}$	volumetric flow rate of air, m^3/s
$\overline{V}$	mean velocity of air in the test channel, m/s
Re_{D_h}	Reynolds number based on channel hydraulic diameter
Re_{d_p}	Reynolds number based on pipe diameter
Sh_o	Sherwood number
Nu_o	Nusselt number for a smooth channel thermally developed flow
$\overline{Sh}_{D_h}$	average Sherwood number
$\overline{Nu}_{Dh}$	average Nusselt number

h_m	local mass transfer coefficient, m/s
$\overline{h}_m$	average mass transfer coefficient, m/s
f_o	friction factor in a smooth channel for fully developed flow
f	friction factor in the test channel across a blockage
TP	thermal performance ratio, defined as $(\overline{Nu}_{Dh} / Nu_o)(f / f_o)^{-1/3}$

CHAPTER I

INTRODUCTION

Efficiency of gas turbines is dependent on the rotor inlet temperature (RIT). Higher RIT implies an increase in the operating temperature of hot gas path components such as the combustion liner, guide vanes and turbine blades. The maximum RIT possible with currently employed cooling schemes is approximately 1900^{o}C, which is above the melting temperature of materials used for turbine blades. In an effort to increase RIT for improved gas turbine efficiency, highly sophisticated cooling schemes are essential alongside better materials solution. Typically, about 5% of compressed air in a gas turbine is used for cooling the turbine blades. The coolant air passes through shaped passages within the blade and exits through arrays of film cooling holes. Different cooling techniques are adopted for heat transfer from leading edge, mid-chord and trailing edge regions of a turbine blade due to the variation in thermal loads on these regions. Commonly used cooling techniques include impingement cooling, rib turbulated cooling, pin-fin cooling and film cooling.

Figure 1 on the following page demonstrates internal and external cooling concepts for turbine airfoil cooling. The focus of current investigation is to study an internal cooling concept for the trailing edge heat transfer. In gas turbine blades, repeated turbulence promoters are cast on the walls of the internal cooling passages to enhance heat transfer. Thermal energy conducts from the external pressure and suction surfaces of turbine blades to the inner zones, and that heat is extracted by internal cooling. Han (1984) identified that the heat transfer performance in a stationary ribbed channel primarily depends on the channel aspect ratio, the rib configuration, and the flow Reynolds number. In general ribs used for experimental studies are square in cross section, with a typical relative rib height of 5-10% of channel hydraulic diameter and a P/e (P being the rib-to- rib spacing and e being the rib height) ratio varying from 7-15 [1].

This thesis follows the style of *ASME Journal of Heat Transfer.*

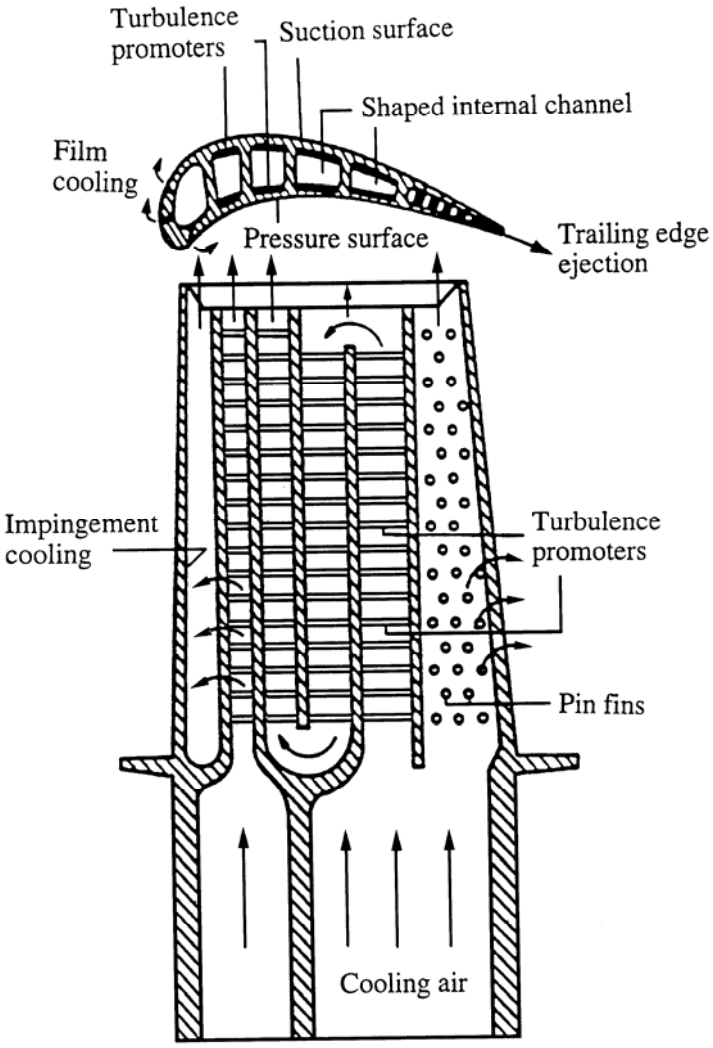

Figure 1: Internal and external cooling concepts used in modern gas turbines

(Han et al. [1])

However, airfoils used in gas turbines do have complicated ribs. For smaller gas turbines, smaller rib spacing and greater rib heights are common.

The objective of this research is to experimentally study a recent cooling design concept for trailing edge heat transfer. In this design, air is forced to flow through parallel blockages having similar cross section as the airfoil trailing edge. Holes in successive blockages are staggered to produce flow impingement and turbulent mixing, leading to better heat transfer from suction and pressure walls of trailing edge. While the previous experimental studies based on this design concept estimated heat transfer enhancement on suction and pressure walls, present attempt is aimed at measuring heat transfer from blockage surfaces to the cooling air. Heat transfer from the blockages is significant because of conduction from the trailing edge surfaces. This added to the fact that cooling air impinges on blockages implies considerable amount of heat transfer from the blockages, in spite of relatively smaller area of convection offered by blockages compared to the trailing edge walls.

Mass transfer experiments were conducted at Re_{Dh} values of 7,000 and 17,000 using naphthalene sublimation technique. Heat & mass transfer analogy was used to determine heat transfer from the blockage surfaces. The test setup consists of a rectangular channel with a cross sectional aspect ratio of 12, a settling chamber or a reservoir, a flow control valve and a pump. Four blockages with different hole configurations, yet with the same total hole area to blockage area ratio were designed. The design facilitated casting of naphthalene in the blockages. For experiments with each hole configuration, the blockage with naphthalene cast in it was inserted along with three other previously fabricated blockages (similar configuration acrylic blockages) into the test channel. While swapping the location of the naphthalene cast blockage with other three acrylic blockages, heat transfer on the blockage upstream and downstream surface at three out of the four blockage locations for a particular Re_{Dh} and hole configuration were determined. Both average and local heat transfer experiments were carried out and

results reported in terms of the ratio of Nusselt number on the blockage surface to the Nusselt number for turbulent flow in a smooth channel. This ratio is a measure of the degree of improvement in heat transfer due to the adopted design.

Low mass transfer rate theory is adopted for estimating the mass convection parameters from the naphthalene sublimation experiments. According to this theory [2], if the gradient in mass fraction of naphthalene (driving potential for mass convection) at the blockage wall surface is less than 0.2, then the mass fraction of naphthalene adjacent to the blockage wall is nearly equal to the rate of naphthalene sublimation. The rate of naphthalene sublimation is estimated using pressure-temperature correlation by Ambrose et al. [3]. Heat and mass transfer analogy is then adopted for estimating the mass transfer Nusselt number (Sherwood number) and other heat transfer characteristics.

CHAPTER II

LITERATURE REVIEW

Cooling techniques commonly employed for gas turbine heat transfer include film cooling, transpiration cooling, and convection cooling with and without turbulence promoters, fin cooling and impingement cooling. Air is chosen over water as the cooling fluid due to corrosion, leakage and fouling problems being associated with water.

Film cooling involves bypassing a portion of compressed air through the combustion chamber wall holes. Hot gases and the bypassed cooling air mix to form a thin layer adjacent to the chamber wall, which protects the wall from high temperature. Experimental investigation of different configurations of combustion chamber wall for mixing of hot gases and cool air have been performed in an effort to improve the performance of film cooling. Film cooling proves to be less effective technique due to its high cooling air requirements. Research indicates that to maintain the combustor wall of a typical turbine at about 1500K, 40% of total mass flow of air is required for film cooling [4]. Transpiration cooling involves permitting compressed cooling air into the combustion chamber through a porous wall in the combustor and this cooling scheme requires lesser amount of air for meeting the same cooling load than film cooling. Suction and pressure surfaces of turbine blades are cooled using film cooling technique while impingement cooling is adopted for turbine blade leading edge and combustor liner wall. Turbulent forced convection cooling is adopted for internal cooling of trailing edge and mid chord region. Extensive research has been done for understanding the turbulent flow and heat transfer characteristics in stationary and rotating channels that approximate the trailing edge or mid chord region, with straight and multi-pass configurations.

Early experiments in rib roughened stationary straight channels included those for square channel, round and annular tubes, and a wide rectangular channel with rib-roughened

walls. White and Wilkie [5] conducted experiments for annular tube with helical rib on the inner wall and a smooth outer wall. Based on Gee and Webb's [6] study of heat transfer and friction characteristics on helically rib roughened tube, among the three different helix angles experimented for a rib pitch to height ratio of 15, the case with 49 degree helix angle was found to give best heat transfer characteristics. Han [7] and Han et al. [8] investigated the effect of transverse and angled ribs on heat transfer characteristics for fully developed turbulent flow in a uniformly heated square channel with square ribs on opposite walls. Results showed those ribs with an angle of attack between 60^o and 75^o enhanced heat transfer and friction most, while ribs with angle-of-attack between 30^o and 45^o gave best thermal performance. Experiments were also conducted by Han and Park [9] for developing and periodically fully developed flows in rectangular channels with aspect ratios of 1, 2 and 4. The dependence of heat transfer and friction roughness functions on channel aspect ratio, rib angle, rib spacing & height, and Reynolds number were studied with foil heater and thermocouple method.

Liou and Hwang [10] employed laser holographic interferometry for studying heat transfer augmentation in rectangular channel for fully developed flows with rib pitch to height ratios of 10, 15 and 20, rib height to hydraulic diameter ratios of 0.063, 0.081, and 0.106, and Reynolds numbers of 5,000 and 54,000. In addition to correlations for average friction factor and Nusselt number, they also presented relative contributions of heat transfer from rib surfaces and exposed surfaces of the channel wall. Similar holographic interferometer experiments were conducted to study heat transfer augmentation for developing channel flow in rib-roughened rectangular channel with abrupt contraction entrance, and for rectangular channel with transverse triangular and semicircular ribs on two opposite walls.

Lau et al. [11] measured the heat transfer and friction factor for turbulent flows in square channels with parallel or crossed arrays of discrete ribs on opposite walls. Rib height to hydraulic diameter ratio and rib pitch to height ratios of 0.0625 and 10 respectively were

chosen for the study and Reynolds numbers of 10,000 and 80,000 were experimented. Results showed that 45^o and 60^o parallel angled discrete ribs were found to cause higher heat transfer and lower pressure drop than 90^o full ribs or 90^o discrete ribs. Also the heat transfer in all the cross-angled discrete ribs was lower than the parallel angled counterpart. From these results, 45^o parallel angled discrete ribs were recommended for internal passage cooling. Further experiments were conducted by Lau et al. [12] to study the effect of aligned V-shaped rib arrays on heat transfer and friction of fully developed turbulent flow in a square channel. Experimental results were obtained for rib angles-of attack of 45^o, 60^o, 90^o, 120^o and 135^o, and rib pitch to hydraulic diameter ratios of 10 and 20. The 60^o V shaped ribs with a pitch to hydraulic diameter ratio of 10 had the highest rib wall heat transfer and smooth wall heat transfer for a given flow rate, and the highest channel heat transfer for unit pumping power. They were found to be superior to 45^o and 60^o full ribs.

Han et al. [13, 14] considered the influence of surface heat flux on heat transfer enhancement in square channel with parallel, crossed and V-shaped angled ribs. Six ribbed wall to smooth wall heat flux ratios and four rib configurtions-90^o ribs, parallel and crossed 60^o ribs and 60^o V-shaped ribs were studied. Results indicated that average heat transfer augmentation on ribbed wall and smooth walls decreased slightly with increasing wall heat flux ratio. Olsson and Sunden [15] conducted experiments to study flows and heat transfer in rectangular channels with parallel ribs, crossed ribs, parallel V-shaped ribs, crossed V-shaped ribs and multiple V-shaped ribs on wider channel walls. For Reynolds number greater than 4,000 it was observed that the ratio of heat transfer augmentation achieved to the additional pressure drop was highest for the case with V-shaped ribs pointing upstream.

Liquid crystal technique was used by Taslim and Spring [16] to study rib profile and spacing effects on heat transfer and friction on the channel walls. Out of the twelve rib geometries and various rib pitch to height ratios, the best case was found to be a rib pitch

ratio of 8 for 90 ^{o} ribs. Several experiments were also conducted to ascertain the contribution of heat transfer form the rib surface to the overall channel heat transfer. 90^{o}, and 45^{o} ribs were studied with staggered rib configurations and with/without the rounding of rib corners. For different geometries tested, ribs with rounded corners had the best thermal performance when the rib spacing was largest and the rib blockage ratio smallest. Several other investigations conducted for rib-roughened channels include studies on triangular channels with rib-roughened walls, trapezoidal channels with tapered turbulators and bleed holes, and rib roughened channels with cross sections of four sided polygons with one semi circular or curve side wall. Delta and wedge shaped turbulence promoters were also investigated by Han et al. [17] for flows in square channels. Chyu et al [18] and Moon et al. [19] found that concavities or dimples on the walls of the channel enhanced heat transfer without large pressure drop compared to the protruding ribs. But further research showed poor performance of such a concept when the inlet air to dimple surface temperature was high.

Kukreja et al. [20] and Lau et al. [21] conducted experiments to measure heat transfer enhancement with different configurations of perforated ribs (constant height to hydraulic diameter ratio of 0.125) for flow through a straight, long square channel. The Reynolds number ranged from 15,000 to 50,000. No improvement in thermal performance was observed with perforated ribs, though the pressure drop across the ribs was lower. There was no improvement in overall heat transfer with varying hole size, number of holes and total hole area.

Moon and Lau [22] studied the effect of staggered blockages (perforated ribs with same cross section as the test channel) with different hole positions and geometry on heat transfer enhancement from the wall surface of a rectangular channel. Experiments were conducted primarily with two blockages in the test channel. The effect of an additional upstream blockage was also investigated. Geometrically similar but different test

sections were used for average and local experiments. The test channels were 35.6 cm long with a cross section of 17.8cm by 3.05 cm. They were connected to a settling chamber, orifice flow meter, gate valve and a blower capable of establishing flow equivalent to Reynolds numbers of 10,000 and 30,000. For measuring the average heat transfer from the channel walls, the portion of wall between two blockages was replaced with a copper plate coated with silicon adhesive on the outer surface. The copper plate was further insulated with Styrofoam and Fiberglass insulation. Thermocouples were installed on the copper plate to determine the average copper plate temperature. For local heat transfer analysis, Inconel thin foil heater with thermochromic liquid crystals sprayed on its inside surface replaced the bottom portion of the channel wall between blockages. A digital camera recorded the temperature contours on heater surface and custom-made software was used to analyze the pictures for temperature distribution.

Different experiments performed include a combination of blockages with centers of holes aligned with and/or offset from the centerline of blockage. Also, experiments were conducted with different hole size and an additional upstream blockage. For the two blockage experiments, it was observed that the heat transfer enhancement was highest for the case (case 2 as per notation in the paper) in which the upstream and downstream blockages had the holes below the respective blockage centerlines. The Nusselt number ratio enhancement was also observed to be high for the case (case3) in which holes in the upstream blockage are below the blockage centerline and holes in the downstream blockage are above the blockage centerline. Also, in case of smaller holed blockages (d=1.27cm), the enhancement of heat transfer in terms of Nu ratio (Nu_{Dh}/Nu_o) was between 5.66 and 8.10 whereas for larger hole case (d=1.91cm), it was between 4.57 and 5.2. The Nu ratios were also observed to be 17% and 36% lower for larger holed blockages with holes on all blockages aligned with the blockage centerline. Local heat transfer experiments indicate higher heat transfer towards the downstream end of wall portion between the blockages and a very low heat transfer at the upstream end. This was a generally observed trend with all the cases. One of the significant conclusions

drawn from the local experiment results was for case 2 (upstream and downstream blockages with holes below the respective blockage centerlines). Local experiment results for this case show no isolated high heat transfer zones and hence rule out possibility of reattachment. High heat transfer in spite of no reattachment was due to vigorous mixing of backflow with the jets from the upstream blockage.

In mass transfer experimental studies conducted by Lau, Cervantes et al. [23] naphthalene sublimation technique was employed to estimate heat transfer enhancement on the test channel walls for flow through blockages with staggered round and square holes. The trailing edge of a turbine blade was modeled as a rectangular channel with approximately same aspect ratio as that of actual trailing edge. The blockages were of the same cross-section as the test channel and the holes in the successive blockages were staggered in order to enhance mixing and thereby, heat transfer from the wall. Experiments were conducted for four different mass flow rates corresponding to the Reynolds numbers of 7000, 14000, 21000 and 28000. Naphthalene cast aluminium cassettes were introduced into the top channel wall and local and average mass losses were measured using depth gage and balance respectively. From this data, all mass transfer and heat transfer parameters were calculated by adopting the heat and mass transfer analogy. Results from average experiments showed that the blockages enhanced the average heat transfer from the channel walls by 4.7 to 6.3 times that for fully developed turbulent flow through a smooth channel. The increase in heat transfer and the pressure drop across a blockage were more pronounced with round holed blockages than with the square holed blockages. As a consequence, the thermal performance of round holed blockages was low. The side of square holes in square holed blockages is the same as the diameter of round holes in the round holed blockages – implying a 27% greater hole area for square holed blockages. Results from local experiments indicate a periodic spanwise distribution of Nusselt number ratio (Nu_{Dh}/Nu_o). This ratio was observed to be higher at the downstream end of the channel wall between any two blockages due to reattachment with the channel wall caused by deflection of air jets. It was also noted that

reattachment occurs only at the downstream tip of the channel wall for round holed blockages, but multiple distinctive high heat transfer regions exist due to reattachment on the channel wall between any two square holed blockages. Other important observation includes the increase in pressure drop by 270 and 490 times that for fully developed turbulent flow through a smooth channel at the same mass flow rate, for round hole and square hole case respectively.

Experimental studies have also been performed with stationary and rotating multi-pass channels. Wagner et al. [24], Johnson et al. [25], studied the surface heat transfer coefficients in rotating multi-pass square channel with normal and angled ribs. Johnson et al. [25] are considered to have done the most systematic investigation of the buoyancy effects and Coriolis forces on heat transfer coefficient distributions of four pass square channels with trips (ribs) angled to the flow. They concluded that the maximum rotating heat transfer coefficient increased 30-40 % compared to stationary 45^o ribbed wall values, while the minimum rotating heat transfer coefficient decreased to 50% of the stationary 45^o ribbed wall model. However, heat transfer coefficient with trip strips was found to be less sensitive to buoyancy effects than with either smooth walls or normal trips. From these results, 45^o angled ribs were recommended over the 90^o angled trip strips. The experiments of Johnson et al. [25] were found to be very close to typical turbine blade cooling conditions and therefore several researchers use their data for comparison.

Considerable progress has been achieved in computational research for analysis of flow and heat transfer in the turbine blade cooling channel. There has also been research on design optimization of rib roughened channel for turbulent heat transfer. This approach by Hong Min Kim and Kwang-Yong Kim [26] presents a numerical procedure to optimize the shape of two-dimensional channel with periodic ribs mounted on both walls to improve heat transfer. Since convective heat transfer of a surface roughened by ribs is significantly affected by flow properties such as reattachment length of the separated

streamline, turbulence intensities and Reynolds number, shape optimization of rib roughened surface should be based on flow structure. In this effort, the authors suggest coupling RANS flow analysis with response surface method for design optimization of channel. Width to height ratio of ribs, rib height- to-channel height ratio, pitch-to-rib height ratio and distance between opposite ribs to rib pitch ratio were chosen as the design variables. Objective function was specified as a linear combination of heat transfer and friction loss related terms with weighing factor.

CHAPTER III

EXPERIMENTAL APPARATUS

The test apparatus consists of an open flow loop in an air-conditioned laboratory. Main components of the flow loop include a test section, a settling chamber, a calibrated orifice flow meter, a gate valve, and a blower. A schematic of the experimental setup is shown in figure 2 and photographs of the experimental setup and instruments used are included in figures 3, 4, and 5.

The test section is 50.8cm (20”) long, the inner cross section is 30.48cm (12”) wide and 2.54cm (1”) high, an inside cross-sectional aspect ratio of 12:1. The test section was made up of 1.27cm (0.5”) thick oak plywood with detachable top wall to facilitate insertion and removal of cassettes. The test section was sealed using Silicone II caulk after inserting the blockages. Four blockages were positioned into the test section with the upstream surface of first blockage at a distance of 26cm (10.24”) from the test section inlet. Each successive blockage is at a distance of 5.08cm (2”) from the upstream blockage. The width of each blockage is 1.14cm (0.45”) and blockage height equals 2.54cm (1”). Successive blockages have staggered holes to enhance mixing and prevent formation of stable thermal boundary layer in the test section. In experiments with any of the four different blockage configurations, three out of the four similar blockages to be inserted into the test section were previously fabricated (of acrylic) while another geometrically similar aluminium blockage, with a cavity for casting naphthalene, was designed and manufactured anew. All blockage configurations have a hole width of 1.27cm (0.5”) and a hole area to channel area ratio of 0.196. Complete design details of blockages are included in chapter IV. The blockages were fixed in the channel using a double-sided tape.

Settling chamber with dimensions of 24” by 15” by 9”, and the test section are connected to the blower using a 2.5” inside diameter PVC pipe. Gate valve and orifice

flow meter were used to control and measure flow rate respectively. Pressure drop across the orifice was determined from the inclined oil manometer. The manometer has a resolution of 0.01 inch H_2O in the 0-3 inches range and resolution of 0.1 inches of H_2O for 3-10 inches range. Temperature at the inlet and upstream of orifice were measured using T type thermocouples calibrated against NIST calibrated mercury thermometer. Air at a temperature of about 25^oC was drawn through the test section and ducted to the outside of laboratory, for all experiments. Data acquisition system was used to read the voltage signals from the thermocouples and output the corresponding data. For average experiments a high resolution Sartorius balance, accurate to one-hundredth of a milligram was used for mass measurements.

For local experiments, Starrett electronic depth gage with a resolution of 0.005" was used and thereby the local elevation of the naphthalene surface before and after the experiment was measured. Naphthalene cast aluminium blockage was positioned on a stage designed to facilitate biaxial movement – a distance of 12 inches in one direction and a distance of 6" in the perpendicular direction. Velmex motion controller was used for moving the stage and measurements of naphthalene surface elevation were taken at 1080 predetermined grid points. The motion of the stage was software controlled using LabVIEW. Effective resolution of the depth gage is higher as a result of combining the data-acquisition system with the Starrett depth gage. The LVDT head of the gage has a range of ±0.2mm and a resolution of 0.0002mm. The additional instrumentation used for local mass transfer experiments is shown in figure 5.

Pressure taps were located mid-way between any two blockages in the test channel. A pressure transducer sends a voltage signal corresponding to the pressure detected to the multimeter. The voltage reading from the multimeter would be converted into the pressure at the location from the pressure transducer calibration data. Calibration of all the thermocouples and pressure transducer was performed before any experiments were conducted.

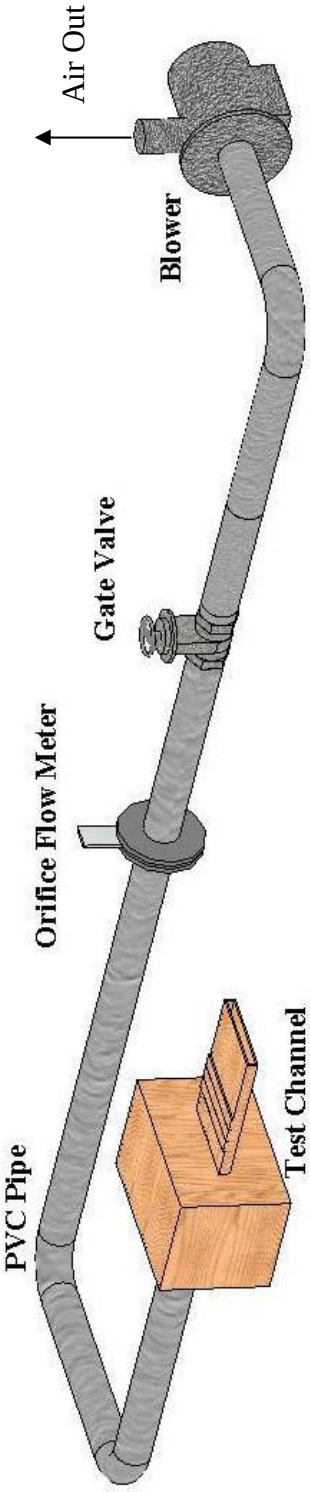

Figure 2: Schematic of test apparatus for mass transfer and pressure measurement experiments

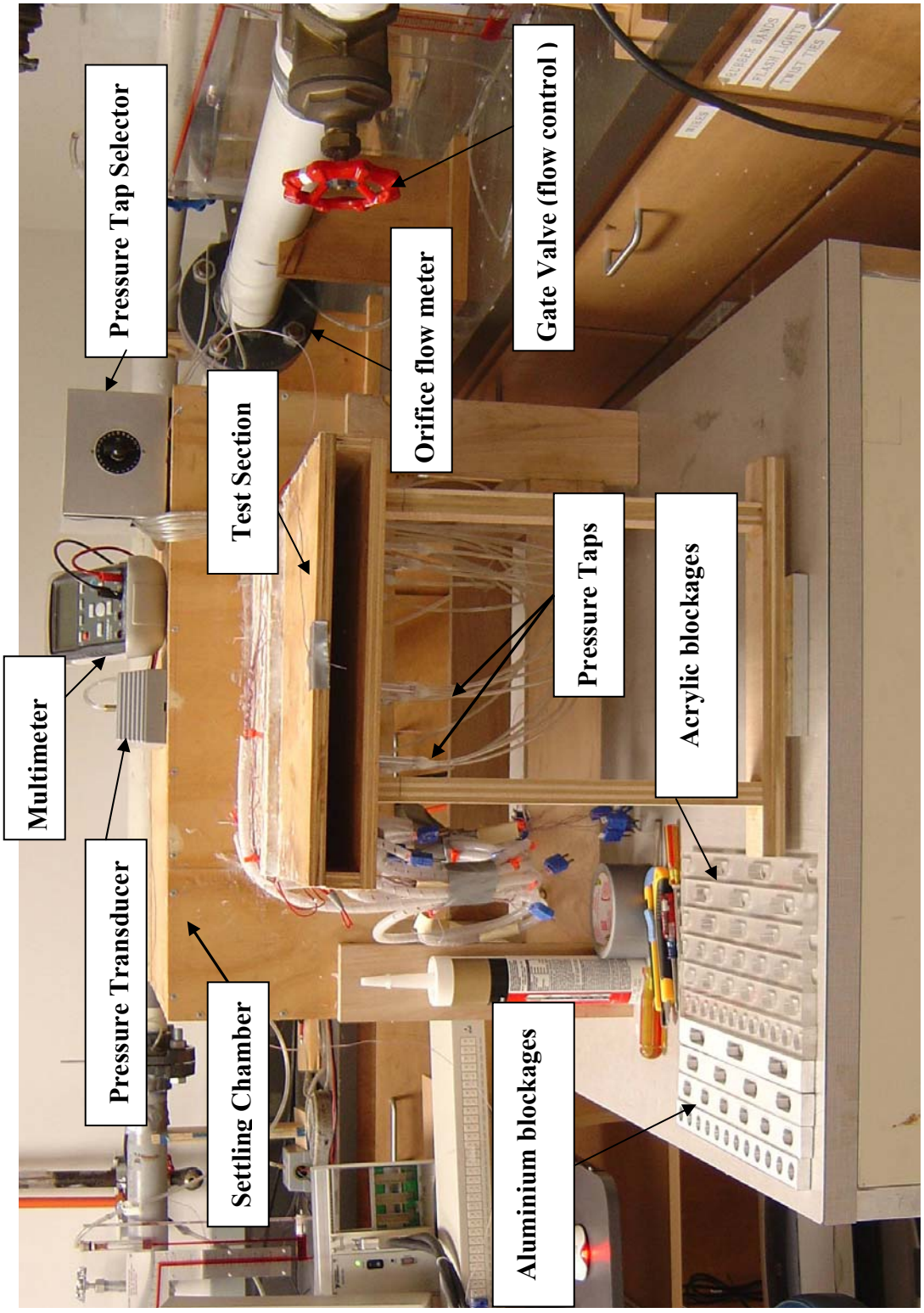

Figure 3: Front view of the experimental setup

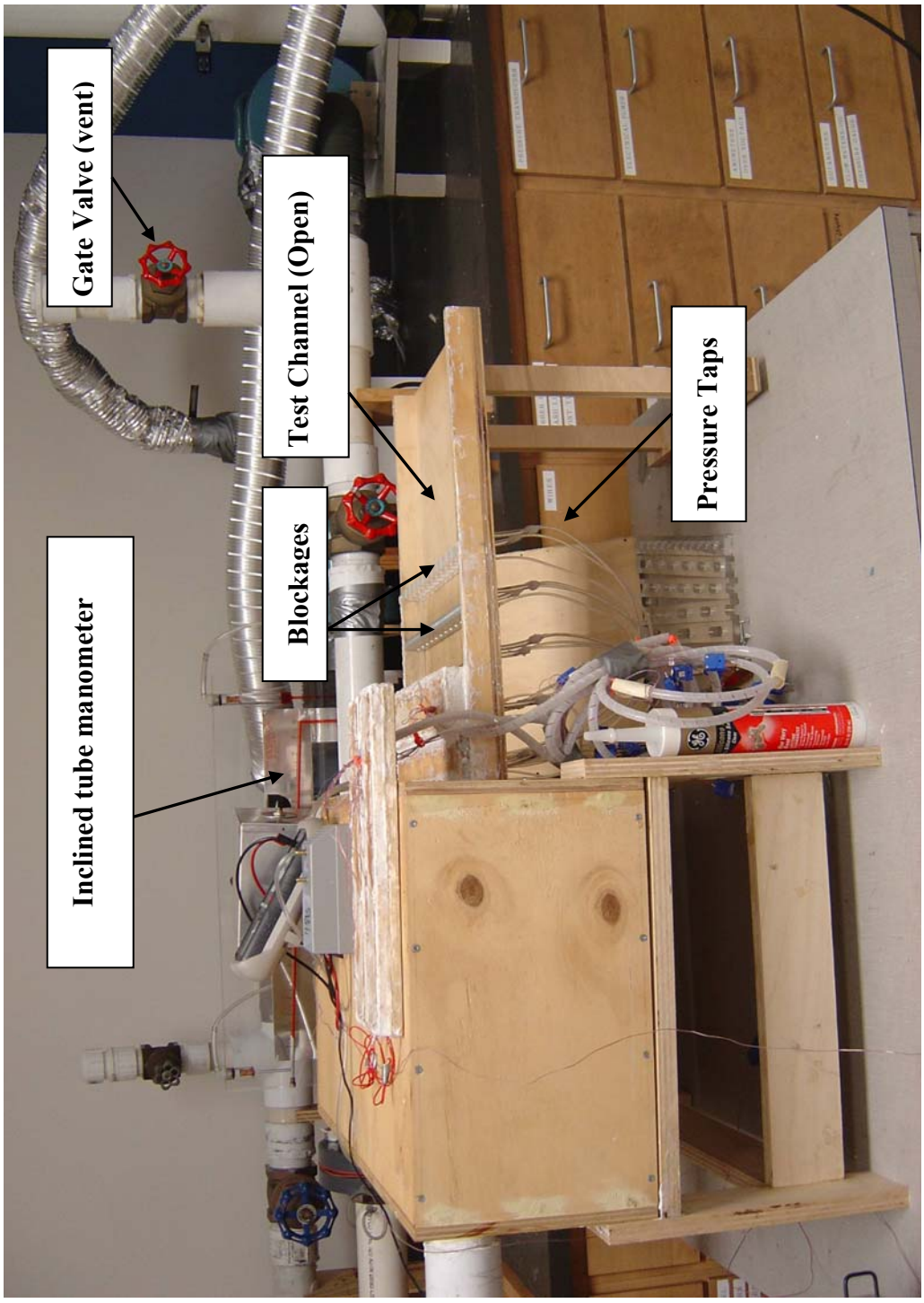

Figure 4: Side view of the experimental setup

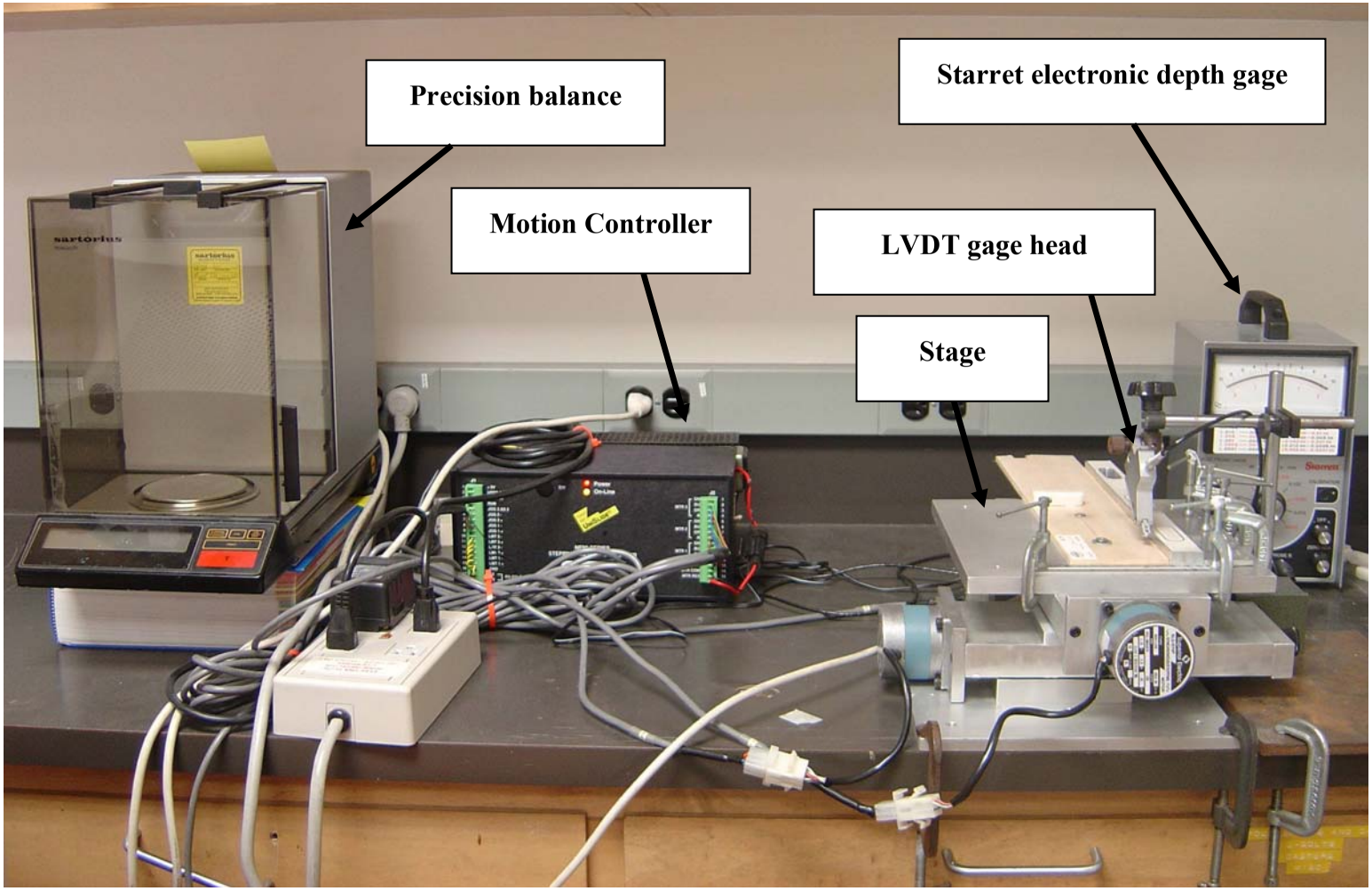

Figure 5: Instrumentation for measurement of local elevation of naphthalene

CHAPTER IV

BLOCKAGES – DESIGN DETAILS

Four different blockage configurations were designed. Primary considerations in the design of blockages were weight of the blockage and mass convection area over the blockage surface. The range of Sartorious high resolution balance is 0-161g. Therefore, blockage configurations were designed to weigh less than 150g with the naphthalene cast in them. Maximum mass convection area over the surface of blockages was ensured by adopting a minimum rim thickness. Minimising the blockage rim thickness further might have posed problems in casting naphthalene into the blockage cavity. All the blockages were manufactured on a CNC machine. Most importantly, the surface finish of the blockage holes was ensured to be very good to avoid roughness contribution by the blockage hole surfaces.

Solidworks drawings of the four blockage configurations are included in the following pages. Figures 6 and 7 represent the first and second blockage configurations. The first blockage configuration has 12 holes of 0.5 inch diameter, while the second blockage configuration has 6 holes of 0.5 inch width and 0.89 inch length. Figures 8 and 9 represent the third and the fourth blockage configurations.

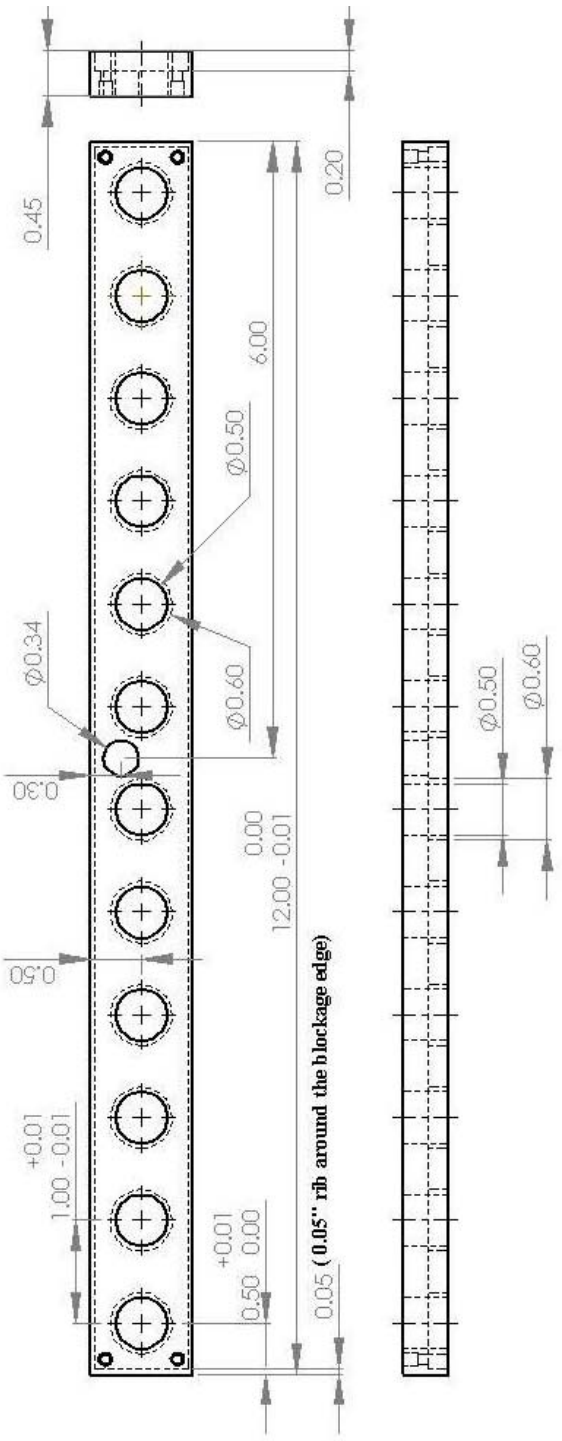

Figure 6: Engineering drawing for blockage configuration 1 (Third angle projection)

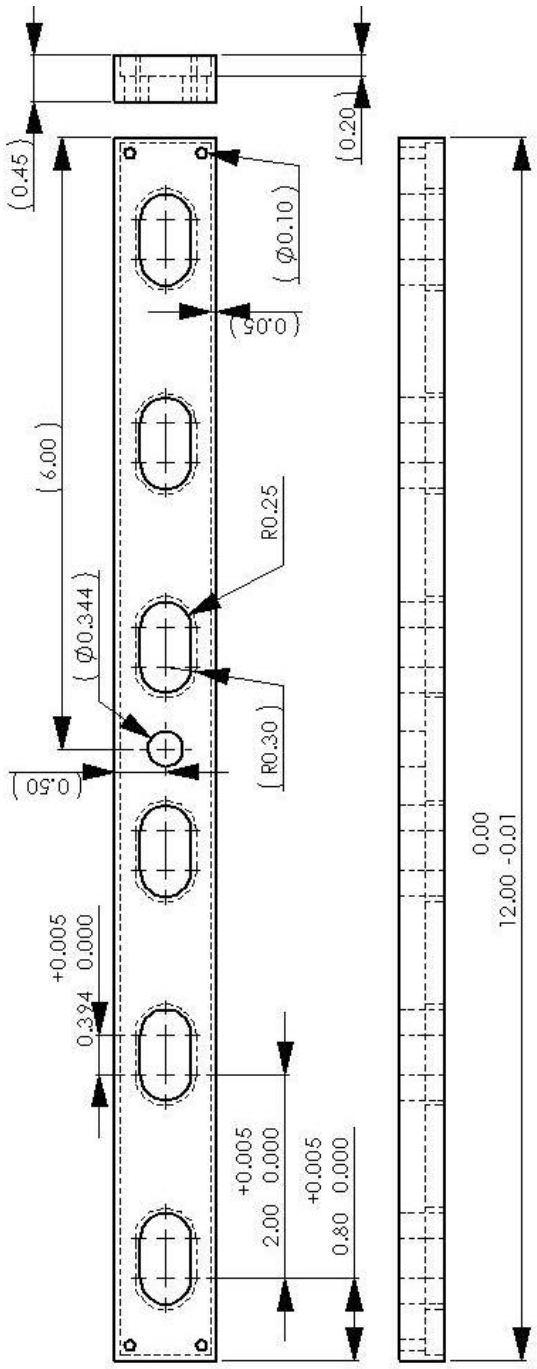

Figure 7: Engineering drawing for blockage configuration 2 (Third angle projection)

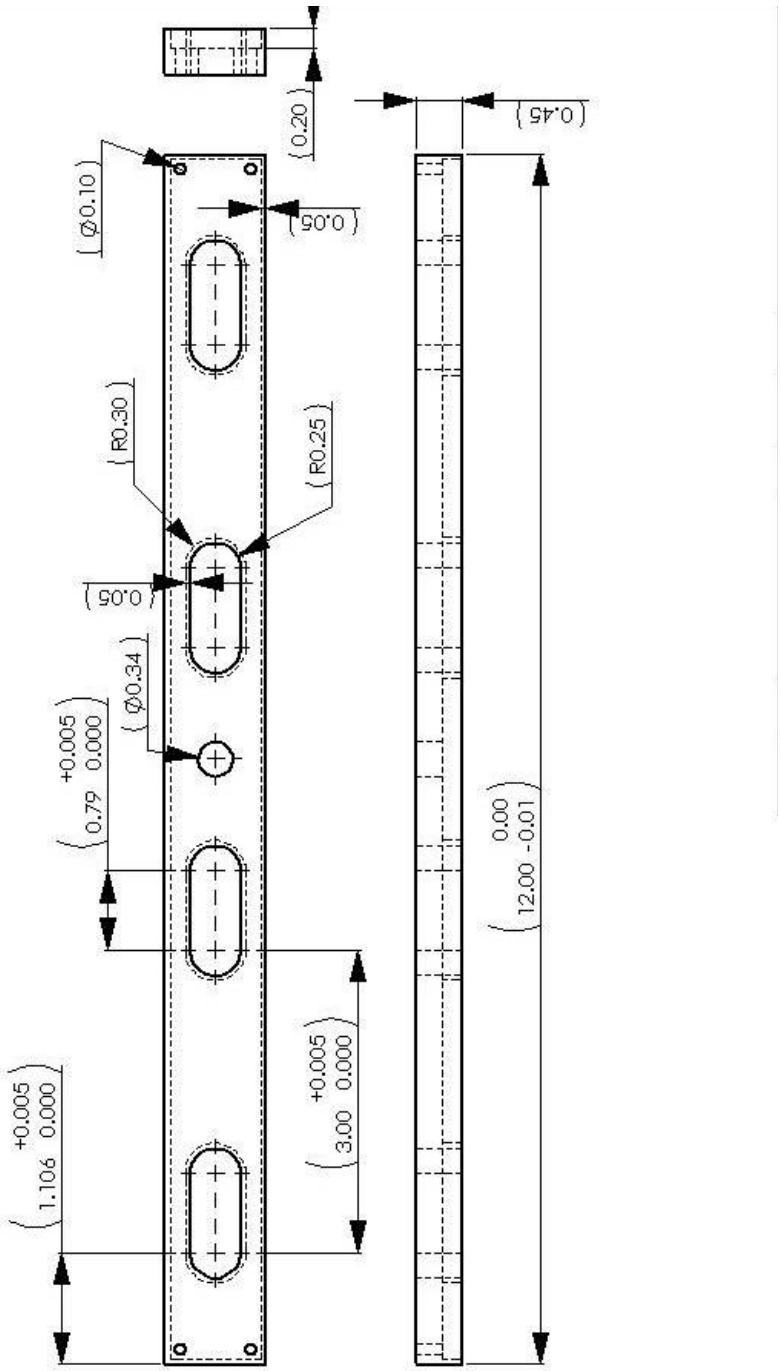

Figure 8: Engineering drawing for blockage configuration 3 (Third angle projection)

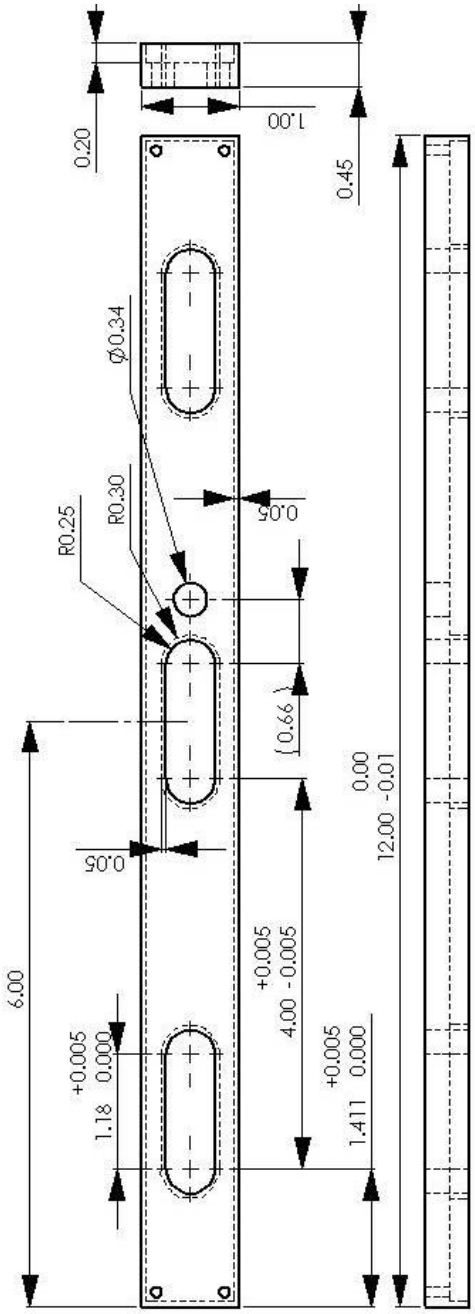

Figure 9: Engineering drawing for blockage configuration 4 (Third angle projection)

CHAPTER V

EXPERIMENTAL PROCEDURE

Naphthalene casting requires a metal surface with good surface finish. A one feet long and half foot wide metal slab was surface ground. This metal slab was used to press aluminium cassette against it. Just before the molten naphthalene was poured into the cassette cavity, cassette and the metal slab were heated slightly. Then the cassette was pressed against the slab, with cassette cavity towards the ground surface, using dead weights. Molten naphthalene heated to about 200^{o}C (though the naphthalene melting temperature is about 85^{o}C, it is heated to this temperature for better flow-ability during casting) was poured into the cavity through the feeder hole in the cassette. Riser holes provided on the cassette facilitate better casting. The cassette was allowed to cool to the room temperature and then was separated from the metal slab by tapping slightly on one side with a hammer. A recasting was done if the naphthalene surface was not satisfactory. In case of local heat transfer experiments, naphthalene inserts were also cast so that the measurement with depth gage was possible.

To ensure thermal equilibrium of naphthalene with air in the laboratory, the cassette was stored in a sealed plastic bag for at least 2 hours and then the experiment was conducted. Before the start of any experiment, gate valve was adjusted to establish flow in the channel corresponding to required Reynolds number.

For average mass transfer experiments, weight of the cassette before and after the test was measured using a balance and the difference in weight (after natural convection and test start up losses are subtracted) was a measure of mass of naphthalene convected at the test conditions. For local mass transfer experiments, local elevation of naphthalene surface was measured using depth gage before and after the experiment and the elevation change data was used to calculate the local mass transfer and heat transfer parameters. Also, from previous research it becomes obvious that the elevation reading for the

traversal of depth gage on the cassette rim before and after experiment may not match. In order to account for this variation, the rim elevation change data was appropriately incorporated into the naphthalene surface elevation.

Every experiment whether local or average experiment was followed up with a test to estimate the losses during the test start-up and ending. The time from blower start-up to the instant the oil in the manometer stabilizes was treated as the start-up time and the loss would be estimated by the auxiliary experiment. The effective duration of an actual experiment was then subtracted from the total experiment time to obtain the time accountable to natural convection. Experiments were also done to establish a relation for natural convection losses with time. Then the total losses (which include the natural convection losses and test start up losses) were subtracted from the total mass convected to obtain forced mass convection during the actual experiment.

Also, in order to estimate the uncertainty associated with the experimental data, all the readings–including pressure, manometer reading, balance reading, and temperature reading were repeated several times over the length of the experiment. Estimation of uncertainty was based on a confidence level of 95% and the relative uncertainty analysis method of Coleman and Steele [27].

Matlab code was developed to automatically select and read the experiment-specific data files, process the data to output the mass transfer and heat transfer parameters along with the Reynolds number, mass flow rate and other specific input data.

CHAPTER VI
DATA REDUCTION

All the equations and the correlations used in determining the heat transfer and pressure drop characteristics for each experiment are listed in this section.

Reynolds number based on pipe diameter is expressed as:

$$\mathrm{Re}_{d_p} = \frac{4\dot{m}}{\pi d_p \mu} \tag{1}$$

In (1), d_p is the internal diameter of the pipe and $\dot{m}$ is the mass flow rate of air given as

$$\dot{m} = 0.25\pi d_o^2 CY\sqrt{(2P_o\Delta P_o)/RT_o(1-\eta^4)} \tag{2}$$

In (2) d_o is the orifice diameter, T_o is the temperature of air upstream of orifice, P_o is the pressure at the upstream section of the orifice, ΔPo is the pressure drop across the orifice, R is the gas constant of air in J/Kg K, T_o is the temperature upstream of the orifice and η is the ratio of orifice diameter to the pipe diameter. C and Y [28] are constants defined as

$$C = 0.5959 + 0.0312\eta^{2.1} + \frac{91.71\eta^{2.5}}{\mathrm{Re}_{dp}} - 0.01584\eta^3 + \frac{0.039\eta^4}{1-\eta^4} - 0.1840\,\eta^8 \tag{3}$$

$$Y = 1.0 - \frac{(0.41+0.35\eta^4\Delta P_o)}{1.4} \tag{4}$$

Equations for $\dot{m}$ and Re_{d_p} are solved simultaneously. Reynolds number based on hydraulic diameter of the test section is calculated as

$$\mathrm{Re}_{D_h} = \frac{\rho\bar{V}D_h}{\mu} = \frac{4\dot{m}}{\mu P} \tag{5}$$

In (5), ρ is the density of air; $\bar{V}$ is the mean velocity of air in the channel; D_h is the hydraulic diameter of the test channel; μ is the viscosity of air; and P is the inside perimeter of the channel.

Vapour pressure $P_{v,w}$ at the naphthalene wall surface is then obtained using the equation by Ambrose et al. [3] shown below.

$$T_w \log P_{v,w} = 0.5a_0 + a_1x + a_2(2x^2-1) + a_3(4x^3-3x); \quad T_w \text{ in K and } P_{v,w} \text{ in Pascal.} \tag{6}$$

In (6), $x = (2T_w-574)/114$, $a_0=301.6247$, $a_1=791.4937$, $a_2 = -8.2536$, $a3 = 0.4043$.

Naphthalene vapour density is calculated as

$$\rho_{v,w} = \frac{P_{v,w}}{R_n T_w} \tag{7}$$

$\rho_{v,w}$ is the naphthalene vapour density at T_w (wall temperature) and R_n is gas constant for naphthalene

Average mass transfer coefficient is calculated as

$$\bar{h}_m = \left(\frac{\Delta M_n}{\rho_{v,w} A_s \Delta t}\right) \tag{8}$$

In (8), ΔM_n is the mass convected, and A_s is the effective area available for mass convection during the experiment.

Local mass transfer coefficient is calculated as

$$h_m = \frac{(\rho_s \Delta z / \Delta t)}{\rho_{v,w}} \tag{9}$$

ρ_s is the solid phase density of naphthalene; Δz is the local elevation change in the naphthalene surface, Δt is the effective experiment duration, and $\rho_{v,w}$ is the density of naphthalene vapor at the blockage wall.

Average Sherwood number is calculated as

$$\overline{Sh}_{Dh} = \frac{\bar{h}_m D_h}{\sigma} \tag{10}$$

σ is the diffusion coefficient given by Goldstein and Cho [29] correlation below

$$\sigma = 0.0681(T_w/298.16)^{1.93}(101325/P_{atm})10^{-4} \quad ; P_{atm} \text{ is taken as 1bar.} \tag{11}$$

$\overline{Nu}_{Dh}$ is calculated from $\overline{Sh}_{Dh}$, using the heat and mass transfer analogy as described in Eckert [30]. This relation (on next page) is valid for Sc >0.5. (In the present case Sc =2.28).

$$\overline{Sh}_{Dh} / Sh_o = \overline{Nu}_{Dh} / Nu_o ; \tag{12}$$

$Nu_o = 0.023\,\mathrm{Re}_{Dh}^{0.8}\,\mathrm{Pr}^{0.4}$; $Sh_o = 0.023\,\mathrm{Re}_{Dh}^{0.8} Sc^{0.4}$; Dittus-Boelter equation [31] (13)

Pr =0.71 for air at room temperature and Sc=2.28 for naphthalene in air at room temperature and atmospheric pressure. Nu_o, Sh_o are based on Dittus-Boelter correlation

Heat transfer coefficient is then calculated as

$$\mathrm{h}= (\overline{Nu}_{Dh}\ \mathrm{K}) / D_h \tag{14}$$

Friction factor ratio for the ribbed channel is determined as

$$\frac{f}{f_o} = \frac{(\frac{2\Delta p}{\rho V^2})}{(0.79\ln(\mathrm{Re}_{Dh}) - 1.64)^{-2}} = \frac{2\rho\Delta p(A_c / \dot{m})^2}{(0.79\ln(\mathrm{Re}_{Dh}) - 1.64)^{-2}} ; \tag{15}$$

Δp is the pressure drop across a blockage, ρ is the density of air, and A_c is the channel inner cross sectional area.

Thermal performance [23] is finally calculated as

$$TP = (\overline{Nu}_{Dh} / Nu_o)(f / f_o)^{-1/3} \tag{16}$$

CHAPTER VII

PRESENTATION AND DISCUSSION OF RESULTS

Results - Average Heat (Mass) Transfer Experiments

Average mass transfer experiments were conducted for turbulent air flow through the test channel (internal aspect ratio of 12:1) with different blockage configurations. The flow was neither hydrodynamically fully developed nor thermally fully developed at any section of the channel. Experiments were conducted at flow rates corresponding to Re_{Dh} values of 7,000 and 17,000. On the basis of low mass transfer rate theory, analogy between heat and mass transfer was used to estimate the heat transfer parameters. Average heat (mass) transfer enhancement ratios and heat transfer coefficients on the blockage upstream and downstream surfaces, friction factor ratios and thermal performances were evaluated for all the experiments.

Experiments were conducted with four different configurations (or cases) of blockages. All four cases had the same hole area to the channel area ratio (0.196). The first blockage case consisted of 0.5" (1.27cm) round holes. The second, third and fourth blockage cases had elongated holes with second configuration containing least elongated holes and fourth configuration containing the holes with largest elongation. Complete specifications of different blockage configurations are available in chapter IV. For each experiment, four similar configuration blockages (one out of these four is aluminium blockage consisting of cast naphthalene) with staggered hole arrays were positioned in the test channel.

For the ease of discussion and presentation of results, a naming convention has been adopted to identify each experimental case. Each case is identified with a number indicating the blockage configuration, an alphabet (a, b, or c) suggesting the aluminium blockage (of same configuration as the other three similar configuration acrylic blockages positioned in the channel) location in the channel, another number to identify

if the experiment has been performed at low (1) or high (2) Reynolds number, and ‘Up’ or ‘Dn’ to identify if the upstream or downstream surface of the blockage is being studied for heat transfer characteristics. For example, ‘1a1Up’ would represent an experiment with first (1) blockage configuration, the aluminium blockage with this configuration positioned at first location (a), low (1) Reynolds number experiment to determine the heat transfer distribution on the upstream (Up) face of the aluminium blockage. Similarly, ‘4b2Dn’ would represent a high (2) Reynolds number experiment with fourth (4) blockage configuration, to study the heat transfer characteristics on the downstream (Dn) surface of the aluminium blockage of this configuration positioned at second (b) location. This notation has been primarily used to list results for each experiment in the appendix section.

Previous experiments with the same test setup established that the variation in heat transfer characteristics beyond the third blockage location is negligible. Hence, heat transfer characteristics at first three blockage locations only were studied, though there are four blockages in the test channel for any experiment. Also, only case 1 and case 4 experiments were conducted to estimate range of Nusselt number ratios at third blockage location, since a trend in Nusselt number ratio similar to that at first or second blockage location was expected with different cases and Reynolds numbers.

For the average mass transfer experiments, mass transfer coefficient (h_m) was calculated based on the amount of naphthalene sublimed during the experiment. Average value of percentage uncertainty for h_m was found to be $\pm 4.99\%$, while the maximum percentage uncertainty in h_m was found to be $\pm 13.80\%$. From the mass transfer coefficient data, average Sherwood number ($\overline{Sh}_{Dh}$), average Nusselt number ($\overline{Nu}_{Dh}$) and average Nusselt number ratio ($\overline{Nu}_{Dh} / Nu_o$) were calculated. Local mass transfer experiments, results of which are discussed in detail in the next section, were conducted for some of the blockage configurations. These local experiments were conducted to serve as

verification against average results and also to provide insights into the variation of flow and heat transfer characteristics with different blockage configurations. Results for Nusselt number ratio through local and average mass transfer experiments show an average variation of 5.06%, while the maximum variation was observed to be 13.05%. Considering that the average percentage uncertainty in Nusselt number ratio from average mass transfer experiments is $\pm 5.56\%$, with a maximum uncertainty value of $\pm 11.74\%$, the variation between the local and the average mass transfer experimental results is acceptable.

Figure 10 shows a plot of average Nusselt number ratio on the blockage upstream and downstream surfaces for different blockage cases (or configurations) at first blockage location and at Re_{Dh} corresponding to 7,000 and 17,000. Several important observations can be made from the figure. At the first blockage location, Nusselt number ratio is highest on the upstream surface of case1 blockage with a value of 6.4 and decreases by about 9.4% to a value of 5.8 for the upstream surface of case 4. A similar trend can also be seen in the plots for Nusselt number ratio at the second and third blockage locations, as shown in figures 11 and 12 respectively. This suggests that a blockage with distributed hole area (case 1) has better heat transfer enhancement on upstream surface than a blockage with concentrated hole area (case 4). The contrary is true on the downstream surface i.e. a blockage with concentrated hole area (case 4) has better heat transfer enhancement on its downstream surface than a blockage with distributed hole area (case 1). This is due to air jet reversal at the downstream blockage and re-impingement on the downstream surface of upstream blockage for the blockage case with concentrated hole area. For case 1 blockages, the jet reversal from the downstream blockage is minimal and there is almost no re-impingement on the downstream surface of upstream blockage. These observations are further verified by the local mass transfer experiments. Another observation that can be made from the Nusselt number ratio plots is that the heat transfer enhancement is lower at higher Reynolds numbers – as has been recorded by several researchers earlier. On an average, for experiments at first blockage

location, Nusselt number ratio at Re_{Dh} value of 7, 000 is approximately 18% higher than that at 17,000. Also to be noted is the fact that Nusselt number ratio on the downstream surface of case 4 blockage is higher than the corresponding upstream value. This is possible only by re-impingement of reversed jet from the downstream blockage.

Comparing figures 10 and 11, it can be seen that the Nusselt number ratio on the upstream surface increases steeply from first blockage location to the second – by over 90% for all blockage cases. Maximum value of Nusselt number ratio observed at second blockage location was 12.4 on the upstream surface of case 1 blockage at low Re_{Dh}. Air drawn (at a rate corresponding to the Reynolds number) through the holes in the first blockage constitutes the primary air jets that impinge on the second blockage. The removal of air in the form of primary jets from the channel section ahead of first blockage establishes in this section a flow (induced flow) that impinges on the first blockage with lesser impingement velocity than the velocity of impingement of the primary jets on the second blockage. Hence the Nusselt number ratios recorded are comparatively higher at the second blockage location.

In the following figures, a diagram is included at the top right corner to identify the blockage location where heat transfer characteristics are being studied. Four parallel blockages with holes are represented in this diagram and the blockage corresponding to the location at which heat transfer is being studied is shaded in black color, while other blockages are represented with common pattern shading. Also, each trend line is identified using ‘Up’ or Dn’ and ‘L’ or ‘H’ in parenthesis. Typically a trend line identified as Up (L) would represent the trend of Y-axis variable on the upstream surface at low Reynolds number (Re_{Dh}=7000). Similarly, Dn (H) would mean that the trend line with this identification shows the variation of Y-axis variable with variation in hole configuration on the downstream surface at high Reynolds number (Re_{Dh}=17,000). Hole geometry for each configuration is also represented just above the X-axis line.

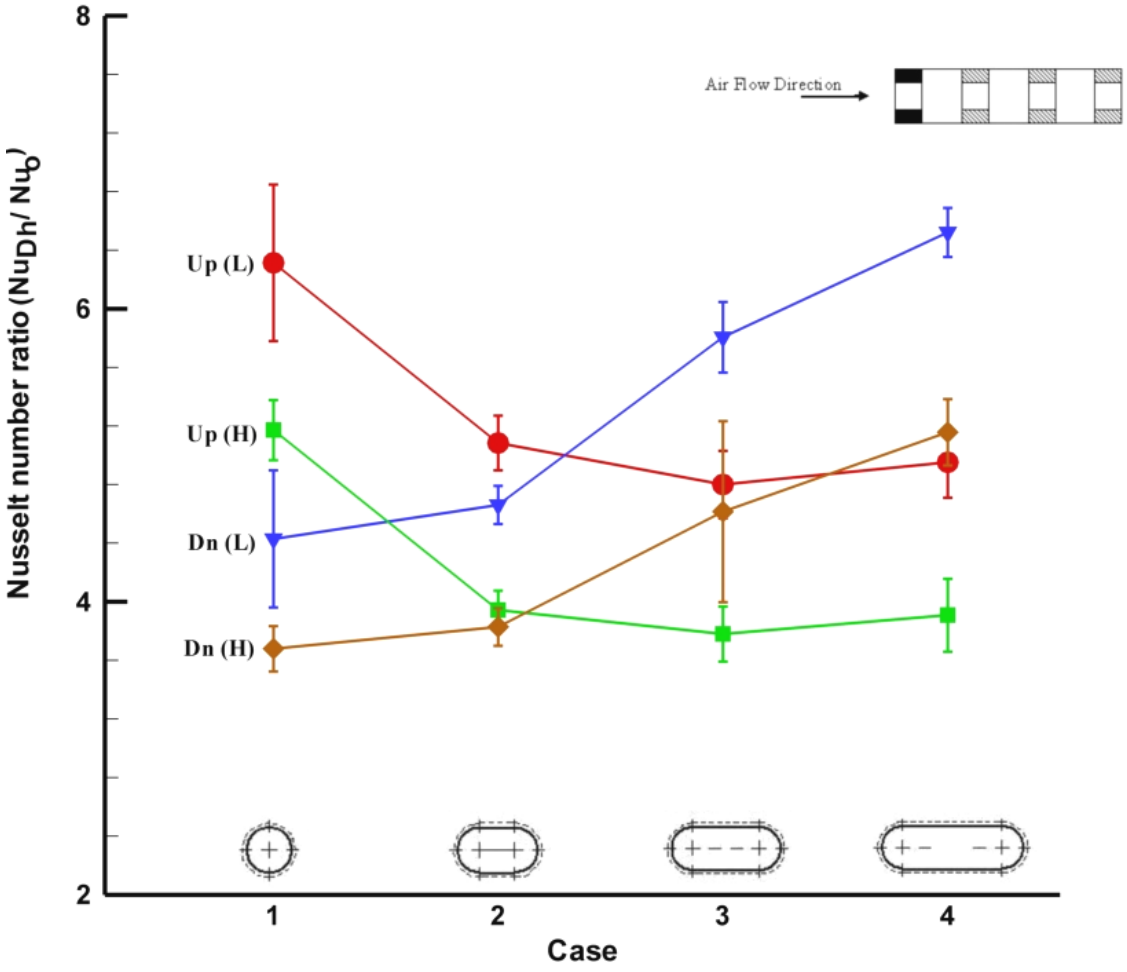

Figure 10: Average Nusselt number ratio for different blockage configurations at the first blockage location

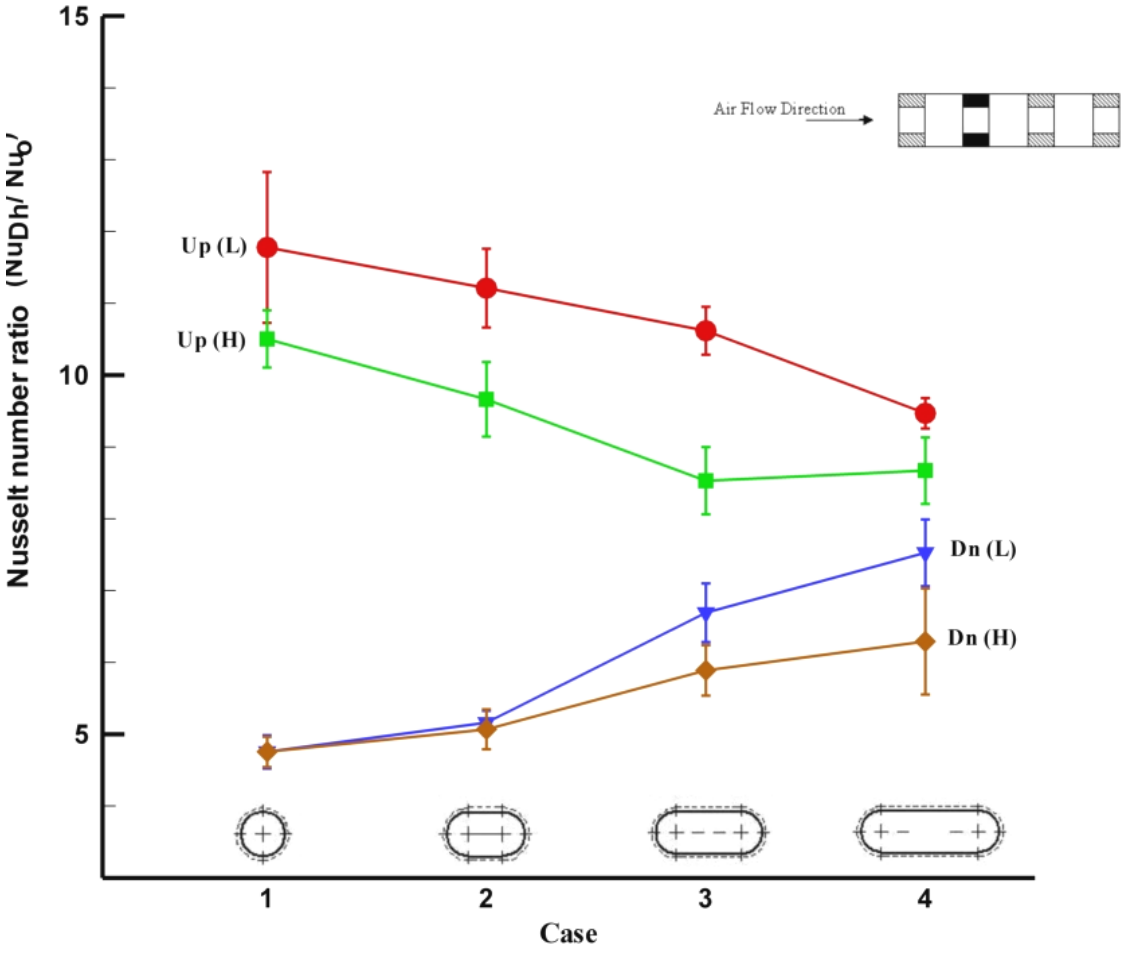

Figure 11: Average Nusselt number ratio for different blockage configurations at the second blockage location

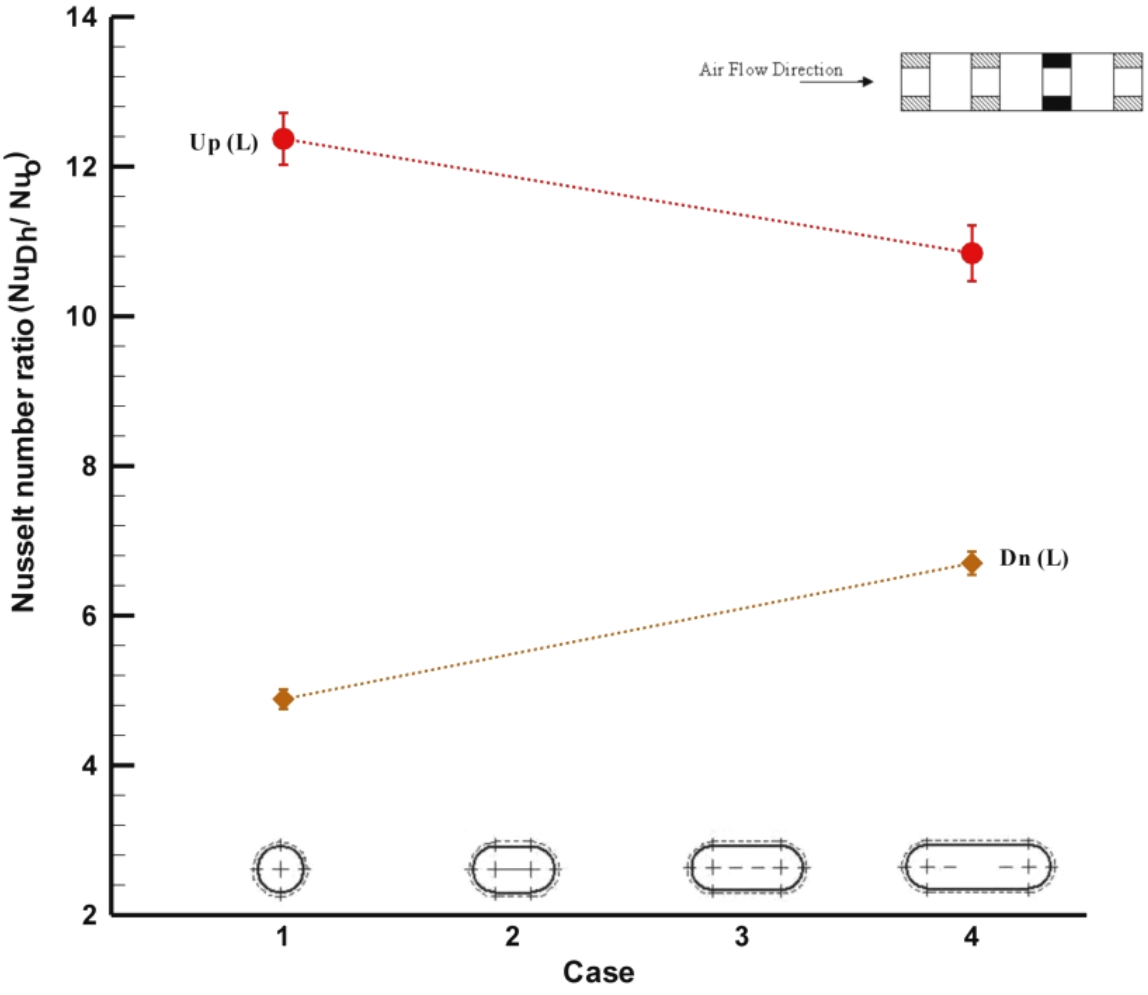

Figure 12: Average Nusselt number ratio for different blockage configurations at the third blockage location

The increase in Nusselt number ratios from first to second blockage location on the downstream surface at first, second and third blockage locations is less prominent - a maximum increase of about 18%. This is because the Nusselt number ratio on the downstream surface of a blockage is determined by flow reversal from the downstream blockage and re-impingement of the reversed air flow. As mentioned earlier, case 1 and case 2 configurations do not lead to significant flow reversal at the downstream blockage and therefore a negligible increase in Nusselt number ratios on the downstream surface, from first to second blockage location, is observed. The flow reversal and re-impingement is observed to be better on downstream surface of second blockage than on the downstream surface of the first blockage for case 3 and case 4. Hence the Nusselt number ratio was observed to be higher at second blockage location than at first blockage location on the downstream surfaces of case 3 and case 4.

Since the heat transfer on the blockage surfaces was due to impingement, results for average Nusselt number observed in these experiments were compared against observations made in earlier work on impingement heat transfer. Important factors in impingement heat transfer include the amount of cross flow established and jet to target plate (impingement surface) spacing. An increase in cross flow has been found to reduce heat transfer from the impingement surface. Also, Sparrow, et al. [32] observed that a jet-to-target plate spacing of 3 jet diameters yielded highest heat transfer coefficients. Goldstein et al. [33] investigated the impingement of a circular jet without cross flow and observed that the maximum Nusselt number was approximately 170, at the center of impingement at a jet Reynolds number of about 35,000. The jet-to-target plate spacing in their research was about 6 jet diameters.

Considering round holed blockages, the jet-to-target plate spacing in the experiments conducted as part of this research was 3.1 times the jet diameter (jet diameter is same as the diameter of blockage holes – a value of 0.5”), close to the value noted in Sparrow, et

al. for maximum heat transfer enhancement. Also, the cross flow is minimal, since the air impinging is drawn downstream through the holes on the impinging blockage. The jet Reynolds number is about 22,300 corresponding to a Reynolds number of 17,000 based on the channel hydraulic diameter. At these conditions, the average value of Nusselt number observed was 503 over the upstream surface of a round holed blockage at second blockage location.

Compared to a maximum Nusselt number value of 170 observed by Goldstein et al. for 35,000 jet Reynolds number, this is almost a three fold increase (Note however that the Nusselt number values are compared for different jet Reynolds numbers and as a result, the actual increase as compared to the value noted by Goldstein et al. will be slightly higher than three-fold).

The three fold increase in Nusselt number as compared to the value noted in Goldstein at al. is due to flow confinement in all directions in the present research unlike in the experiments conducted by Goldstein et al.

Heat transfer coefficient and thermal performance curves also show similar trends as the Nusselt number ratio at all three blockage locations. Figures 13, 14 and 15 show the average heat transfer coefficient plots at first, second and third blockage locations respectively. Heat transfer coefficient at the first blockage location for different cases ranges between 60 - 140 W/m^2K. At the second blockage location, the variation is between 60 - 285 W/m^2K. The maximum uncertainty in heat transfer coefficient was found to be $\pm$ 14.6% while the average value of uncertainty (average of uncertainty over all experiments) was $\pm$ 8.03%.

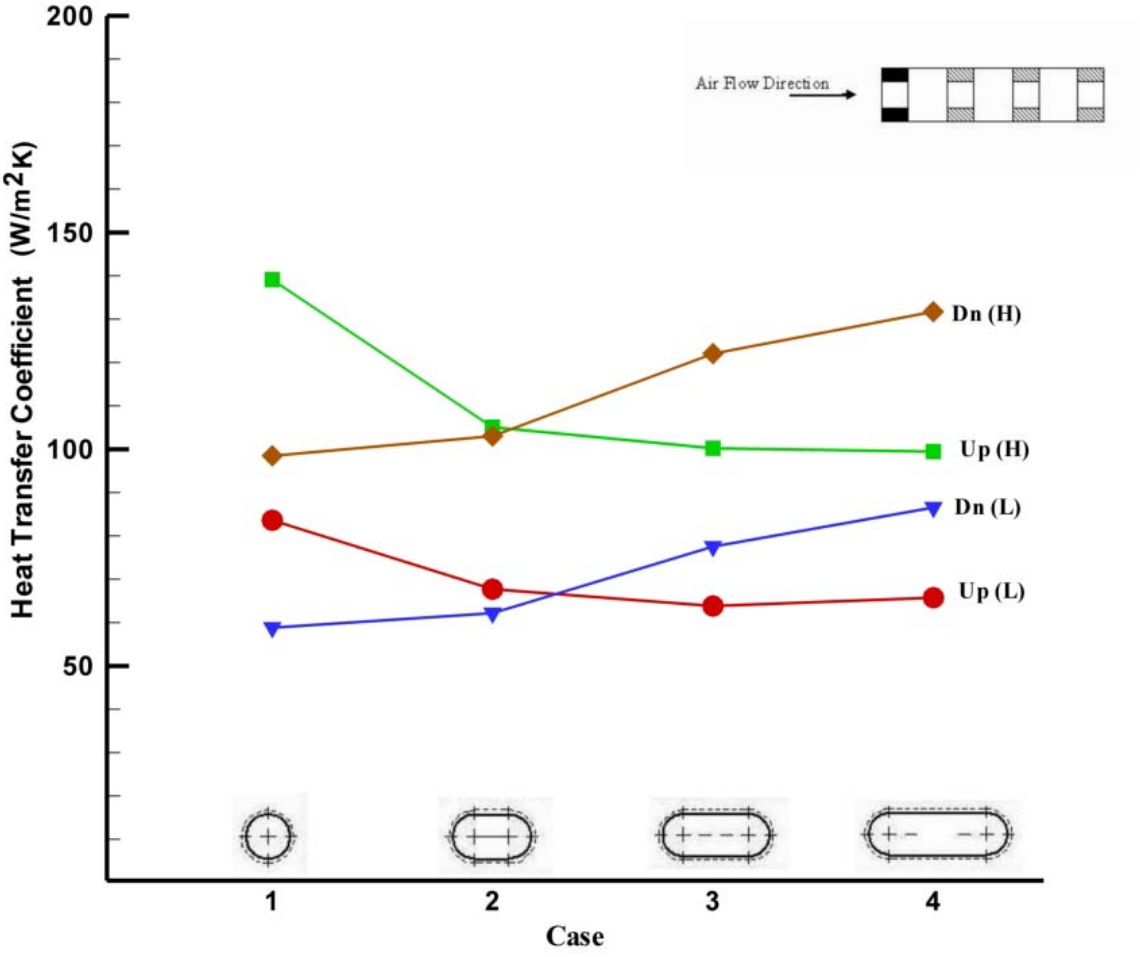

Figure 13: Heat transfer coefficient for different blockage configurations at the first blockage location

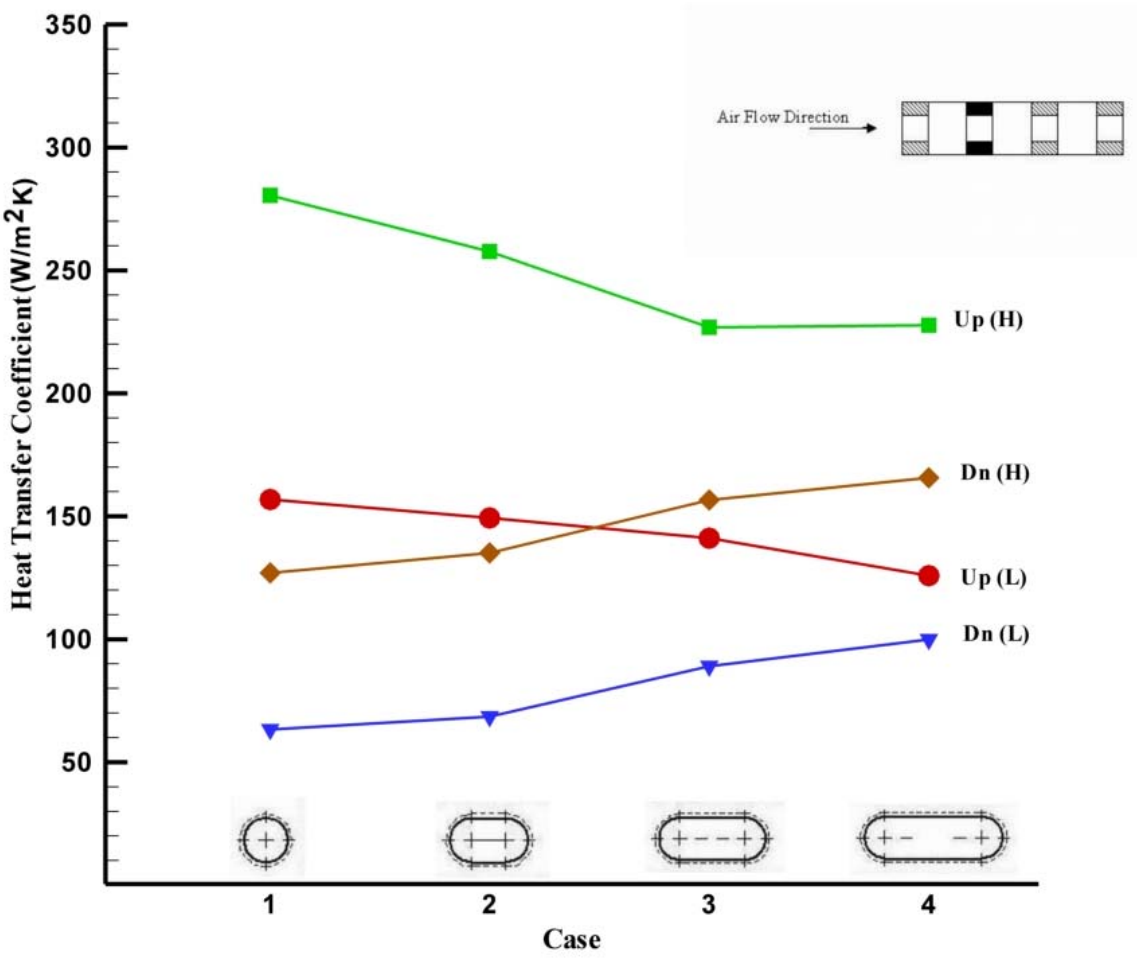

Figure 14: Heat transfer coefficient for different blockage configurations at the second blockage location

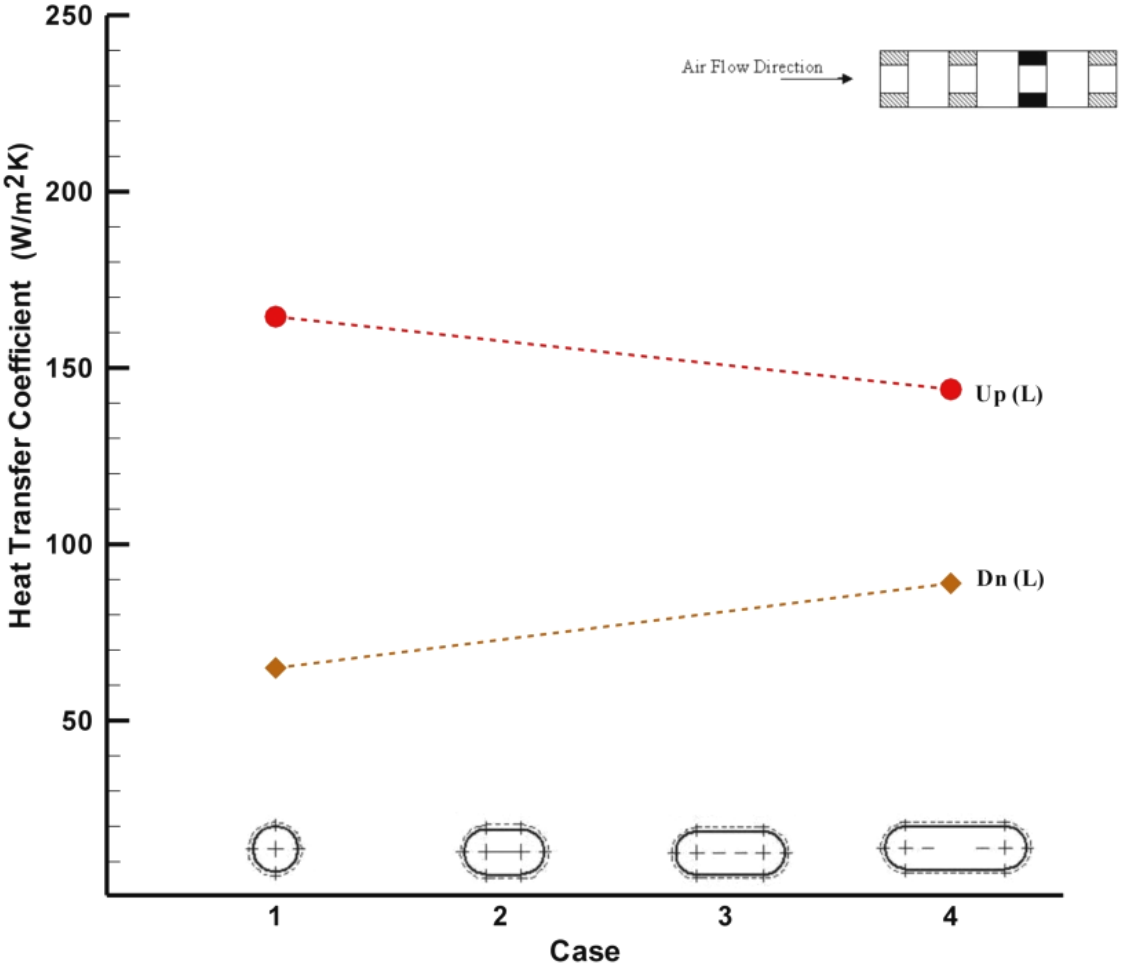

Figure 15: Heat transfer coefficient for different blockage configurations at the third blockage location

Thermal performance plots are shown in figures 16, 17 and 18. Previous work on turbine blade channel cooling by several researchers indicates that rib-turbulated cooling reduces the thermal performance of the channel to a value less than one. In this regard, it should be noted that the thermal performance in previous works was calculated based on the average Nusselt number on the channel wall rather than on the blockage (or rib). Since the flow directly impinges on the blockage, higher Nusselt number ratios and heat transfer coefficients have been observed compared to those observed for the channel wall heat transfer. It also should be noted that thermal performances calculated for blockage heat transfer are only for quantitative comparison. The area weighted average of average Nusselt number ratios for channel wall and the blockage would be representative of the true Nusselt number ratio for the channel. This area weighted average should be used for computing the thermal performance of the channel, since the pressure drop used for thermal performance evaluation is due to both wall friction and the turbulence generated due to the blockages. If the average of upstream and downstream side thermal performances is compared for each case, Figures 16-18 indicate that case 1 blockages result in best thermal performance irrespective of blockage location or Reynolds number. Case 4 is nearly equal but lesser in average (average of upstream and downstream value) thermal performance than case 1.

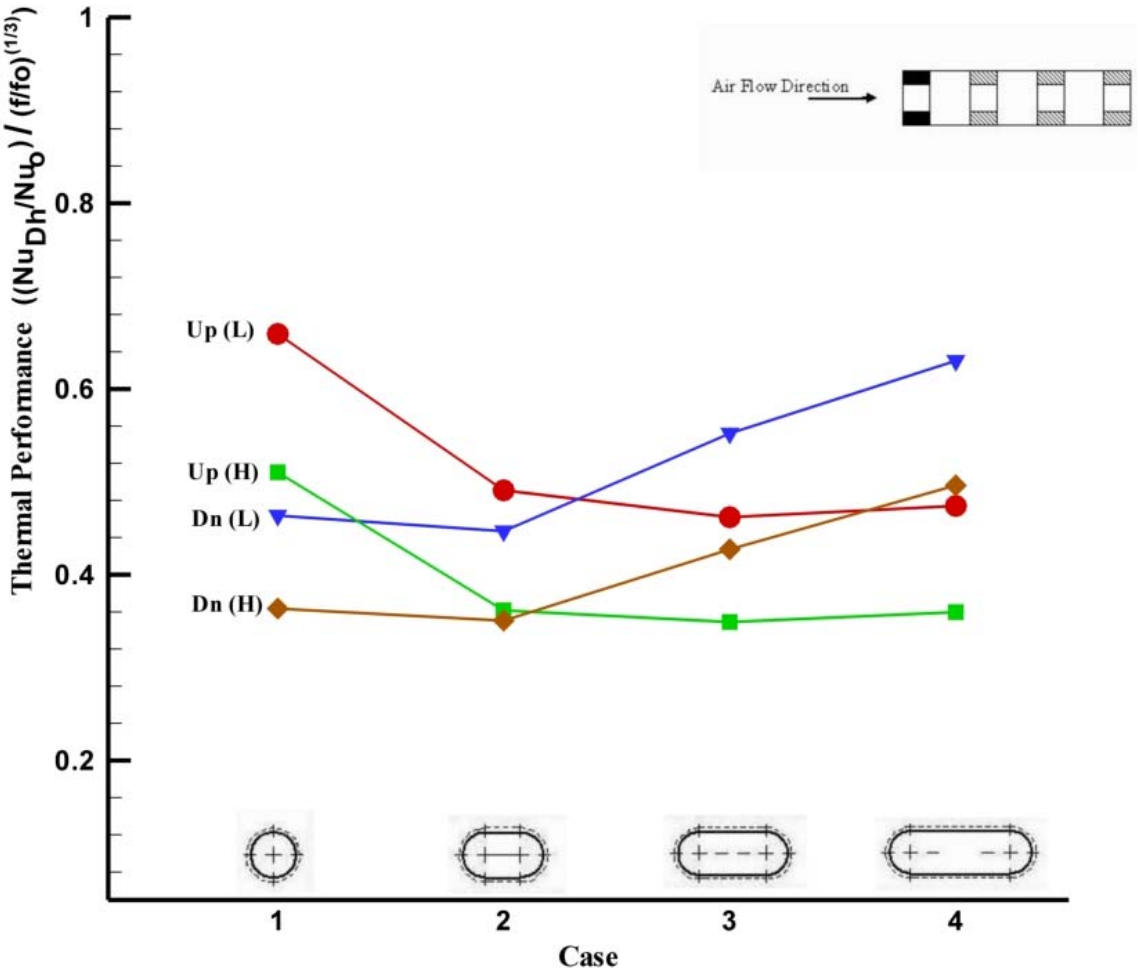

Figure 16: Thermal performance for different blockage configurations at the first blockage location

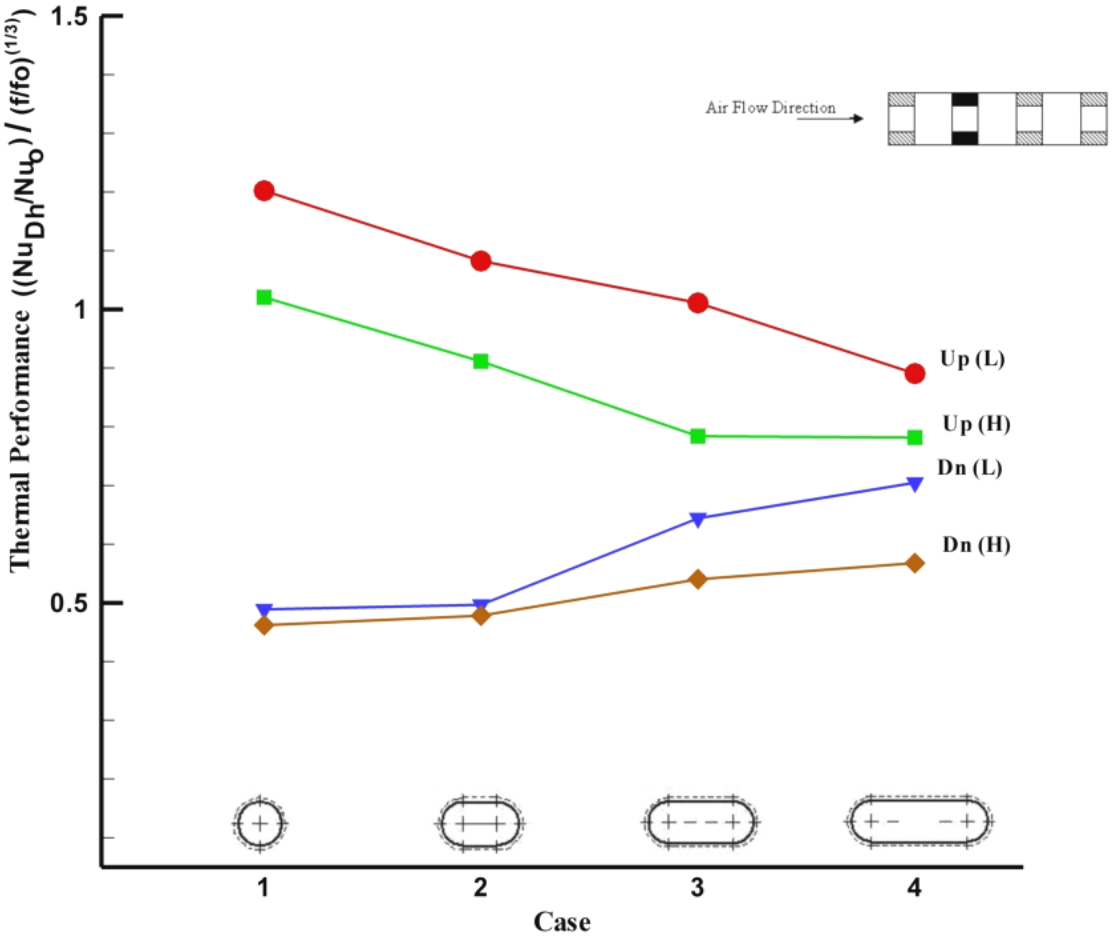

Figure 17: Thermal performance for different blockage configurations at the second blockage location

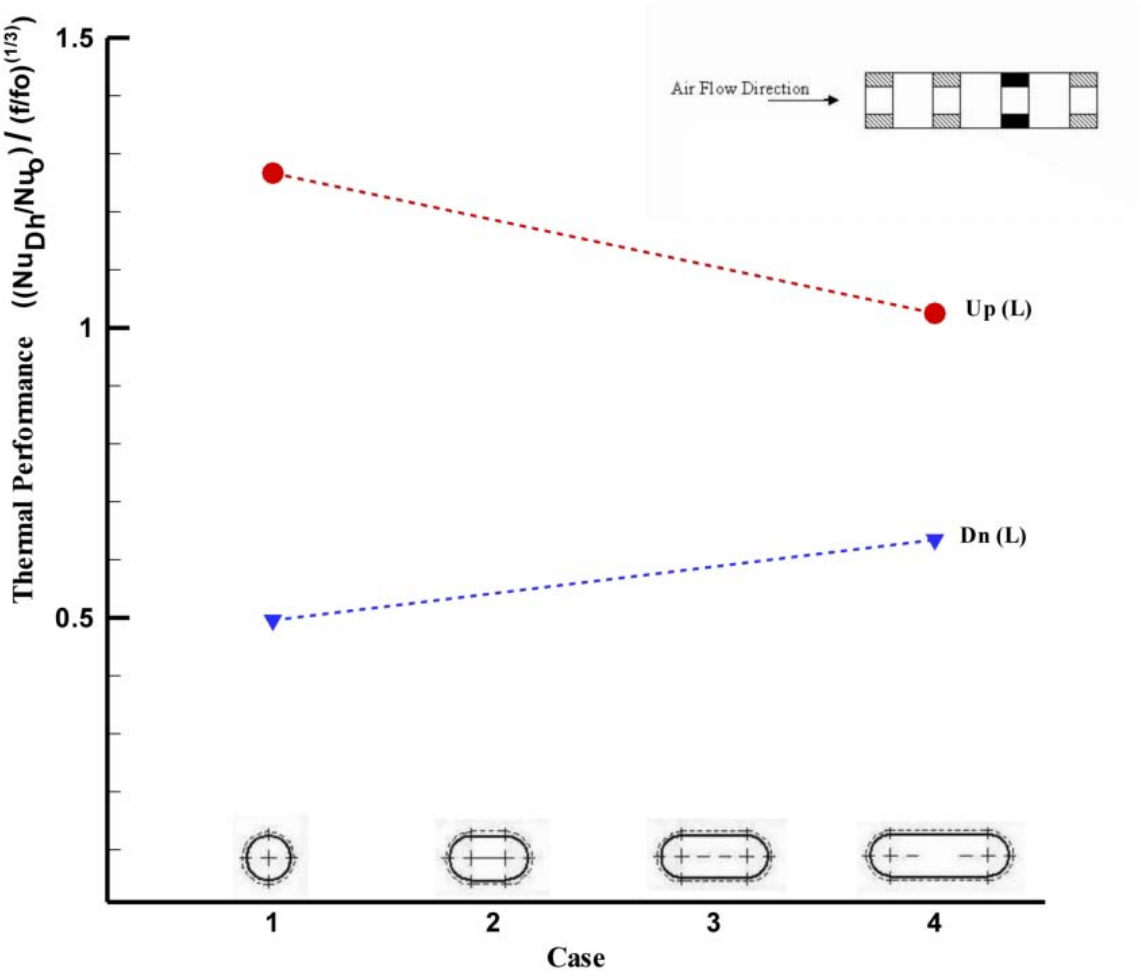

Figure 18: Thermal performance for different blockage configurations at the third blockage location

Three pressure taps were located midway between any two blockages. Three more pressure taps were located in front of the first blockage and behind the last blockage. All the pressure taps were connected using flexible pipes to a pressure channel selector that in turn is connected to a Cole Parmer pressure transducer. The voltage output from the transducer was read out using a multimeter. From the pressure calibration chart, absolute pressure at each pressure tap location was calculated. From this data, pressure drop across any blockage and thereby the friction factor ratio was computed. The maximum value of uncertainty in friction factor ratio was $\pm 8.3\%$ while the average value of uncertainty was $\pm 4.51\%$. A plot of friction factor ratio, defined as the ratio of friction factor for the experiment to the friction factor for a smooth channel fully developed turbulent flow, for all the experiments across first, second and third blockage locations is shown on the following page.

Figure 19 represents trends in friction factor ratio. It is primarily intended to represent the variation of friction factor ratio for a particular case with blockage location and not exactly for comparison amongst different cases. From figure 19, it can be seen that the friction factor ratio increases with Reynolds number. Friction factor ratio at first blockage location is lowest for case 1, with a value of about 880 at Re_{Dh} value of 7,000 and 1,050 at 17,000 Re_{Dh}. Case 2, Case 3 and Case 4 experiments show an almost same friction factor ratio, a value of 1120 at Re_{Dh} value of 7,000 and a value of 1280 at17,000 Re_{Dh}, across first blockage location. In general friction factor should decrease in the downstream direction and the same trend was observed for cases 1 and 2. By their configuration, case 3 and case 4 have a concentrated hole area, as a result of which better mixing phenomenon is in place as compared to cases 1 & 2. Better mixing leads to a greater pressure drop which is reflected in the friction factor for case 3 & case 4 blockages.

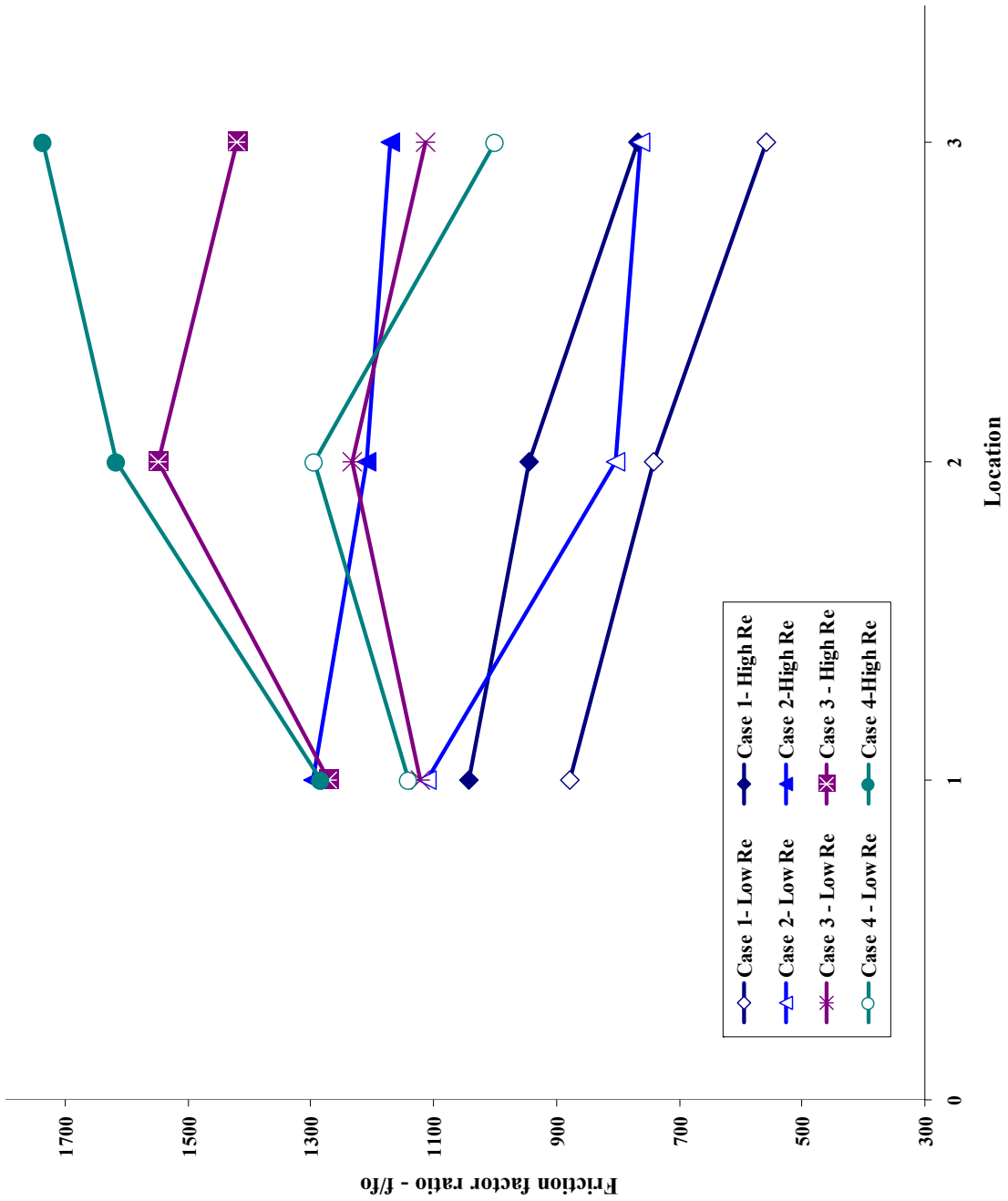

Figure 19: Friction factor ratio at different blockage locations and for all four blockage configurations

Results - Local Heat (Mass) Transfer Experiments

Local heat (mass) transfer experiments were performed for case 1 and case 4 blockage configurations. At the first blockage location, the local Nusselt number ratio was fairly constant over the blockage upstream surface for case 1. This suggested that the variation in heat transfer characteristics over the blockage surface would not be significant with other cases too at first blockage location. Since the interest was to study the spanwise and height-wise variations in heat transfer characteristics on the blockage surfaces, no further local heat transfer experiments were conducted at the first location.

Local mass transfer experiments with naphthalene cast blockage at second blockage location were conducted for low and high Reynolds numbers with case 1 and case 4 blockage configurations. Heat transfer and fluid flow behaviour data was obtained through these local experiments. In order to compare the local heat (mass) transfer experimental results with those from the average heat (mass) transfer experiments, area weighted average of local Nusselt number ratios was determined. There was good agreement between the results from local and average experiments as mentioned earlier in this document.

For local experiments, a motion controller, an electronic depth gage, and a stage to affix the naphthalene cast blockage were used in combination to measure the elevation of naphthalene surface at 18 by 61 pre-determined, equally spaced grid points. The elevation change was recorded by measuring the naphthalene surface elevation before and after the experiment. Flow over a blockage surface is symmetrical about a plane perpendicular to the longest edge of the blockage. Hence the elevation change was measured only for half the span of a blockage and results were extended to represent the full blockage span wherever a comparison between average and local experiments necessitated.

The elevation change data along with other raw data for an experiment (pressure drop across orifice, pressure drop across each blockage, ambient air temperature, etc) was read using a Matlab program and the output matrix containing the local Nusselt number ratios was exported into the database of a post-processing package (Tecplot). Tecplot figures representing the local Nusselt number ratio distribution on the blockage surface are shown in pages 48-56.

From figure 20, the Nusselt number ratio distribution on the upstream surface for case 1 blockage at flow Reynolds number of 7,000 and positioned at first blockage location is fairly uniform.

In all the local Nusselt number ratio plots on the following pages, a diagram is included (to the right corner on the landscaped figure) to identify easily the blockage surface and location where heat transfer characteristics are being studied. Out of the four blockages represented in each of these diagrams, the blockage shaded in black represents the location of interest for the plot and an arrow at this blockage location represents whether the upstream or downstream surface is the surface of interest for studying heat transfer characteristics.

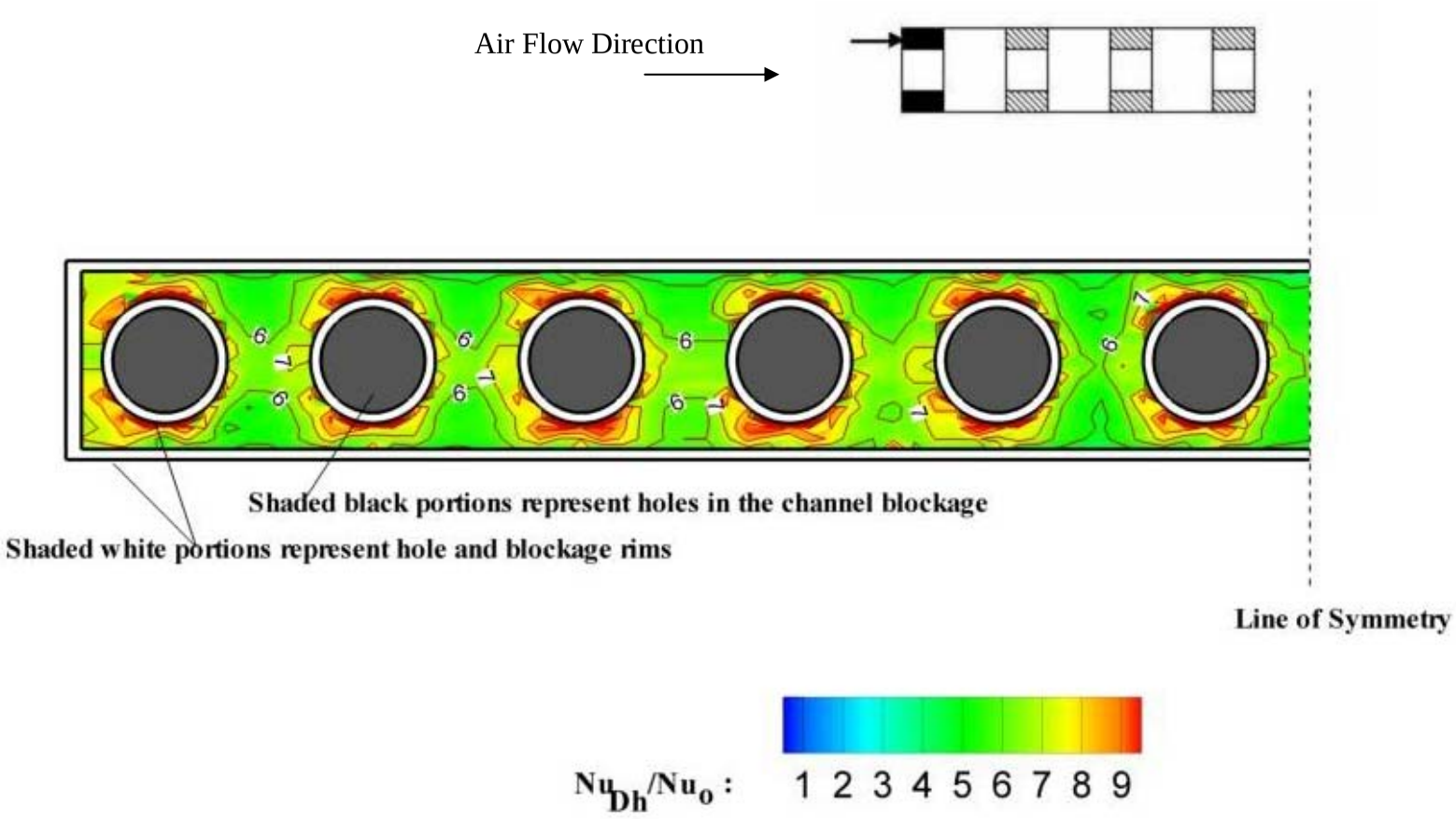

Figure 20: Distribution of Nusselt number ratio, at a Reynolds number of 7,000, on the upstream surface of a round holed blockage (case 1) positioned at the first blockage location in the test channel

Figures 21 and 22 represent the Nusselt number ratio distribution, at flow Reynolds number of 7,000 on the upstream and downstream surfaces for case 1 blockage at second blockage location.

Maximum Nusselt number ratio of approximately 16 was observed on the upstream surface at regions where the primary air jets from upstream blockage impinge. Repetitive pattern is also observed in the Nusselt number ratio distribution over the blockage surface. From the Nusselt number ratio plot for the downstream surface, it can be seen that there are no zones of high heat transfer (Nusselt number ratios comparable to the maximum value on the upstream side) between any two rim holes. This suggests that there is no significant jet reversal at the downstream blockage and hence no re-impingement of air jets on the downstream surface of upstream blockage. Small repetitive regions of high heat transfer towards the top and bottom ends of the blockage on the downstream surface are representative of secondary flows.

At high Reynolds number (Re_{Dh}=17,000) for case 1 blockage at second blockage location, the maximum Nusselt number ratio on the upstream surface was found to be approximately 14. Figures 23 and 24 represent the local Nusselt number ratio distribution at high Reynolds number for case 1 blockages.

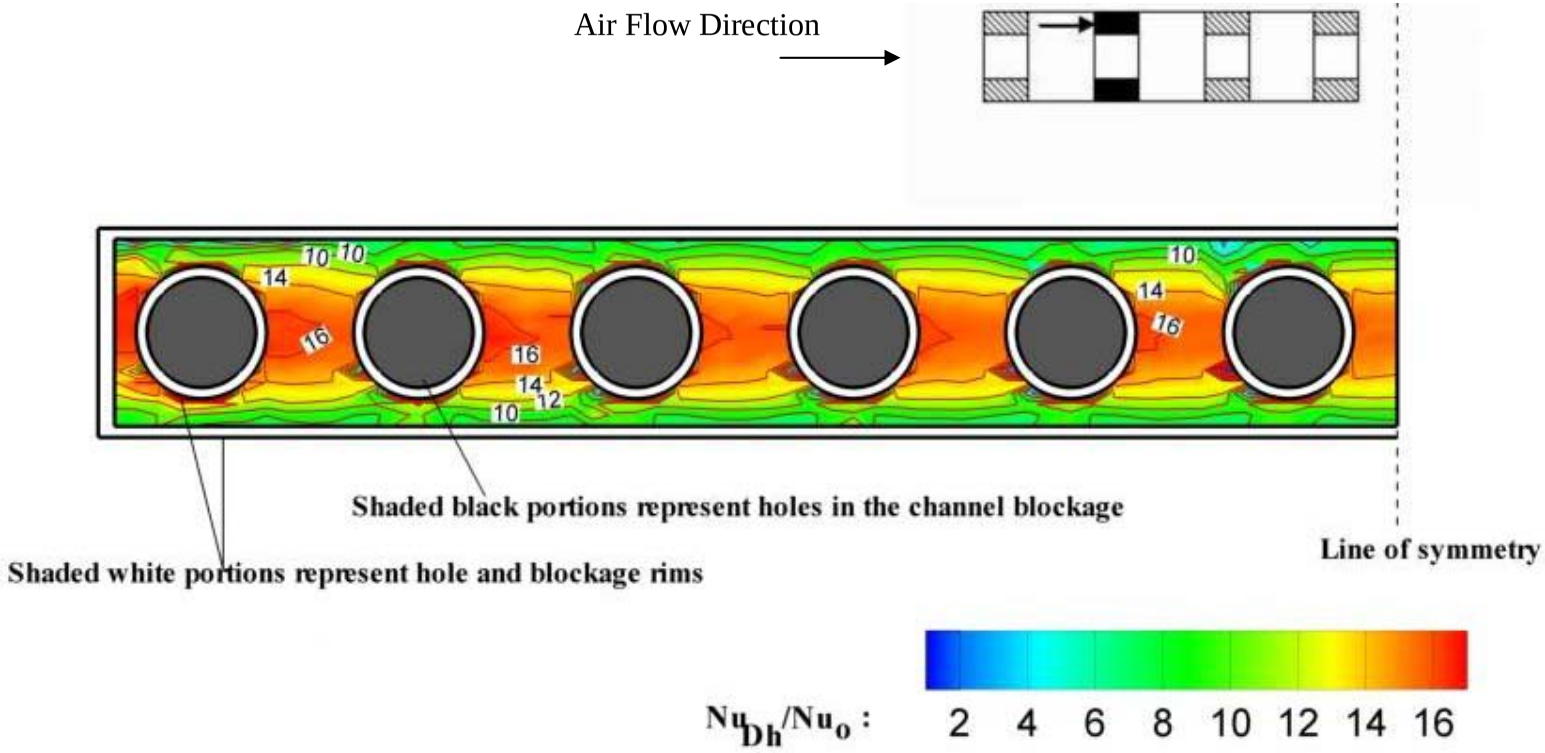

Figure 21: Distribution of Nusselt number ratio, at a Reynolds number of 7,000, on the upstream surface of a round holed blockage (case 1) positioned at the second blockage location in the test channel

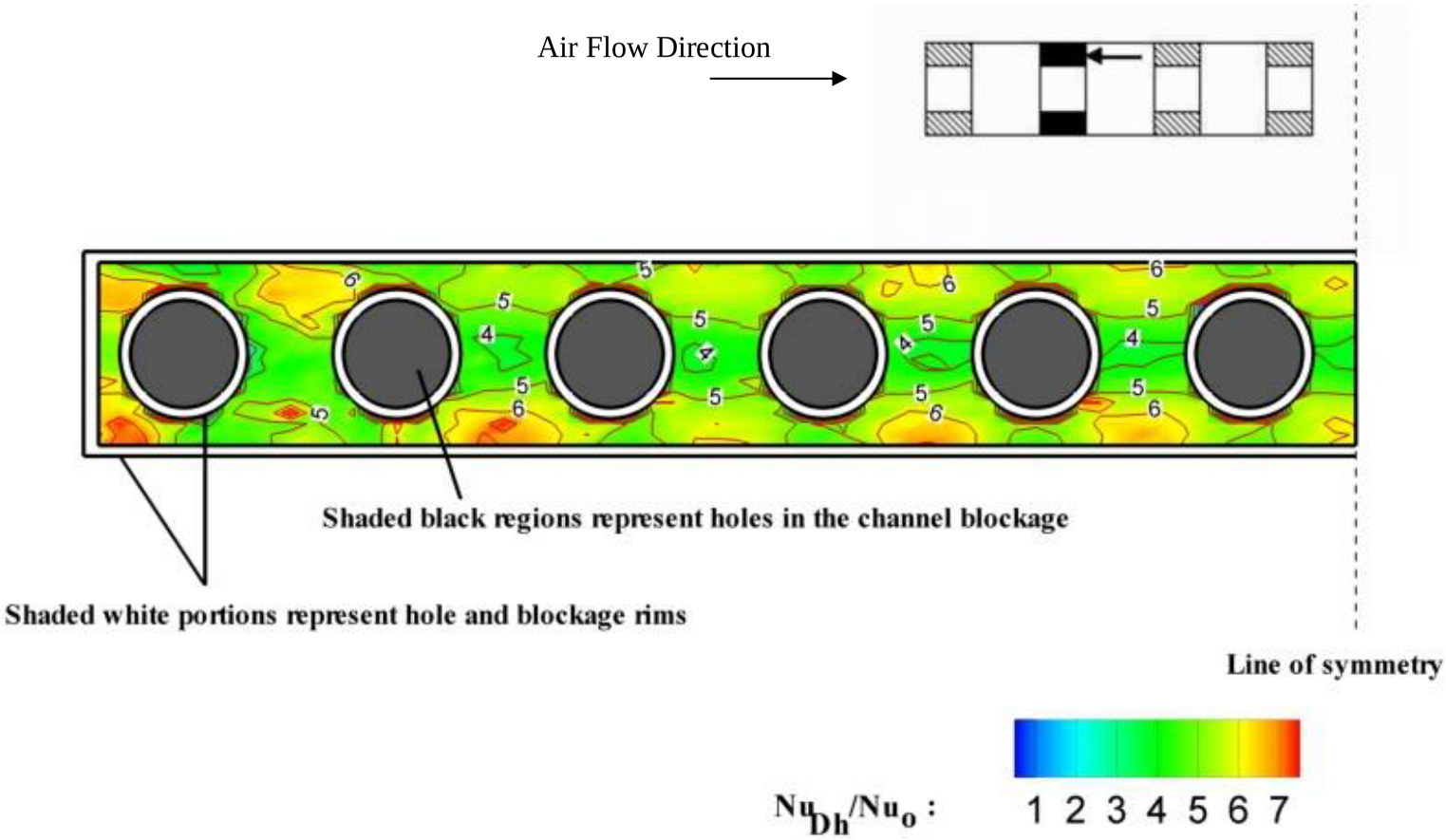

Figure 22: Distribution of Nusselt number ratio, at a Reynolds number of 7,000, on the downstream surface of a round holed blockage (case 1) positioned at the second blockage location in the test channel

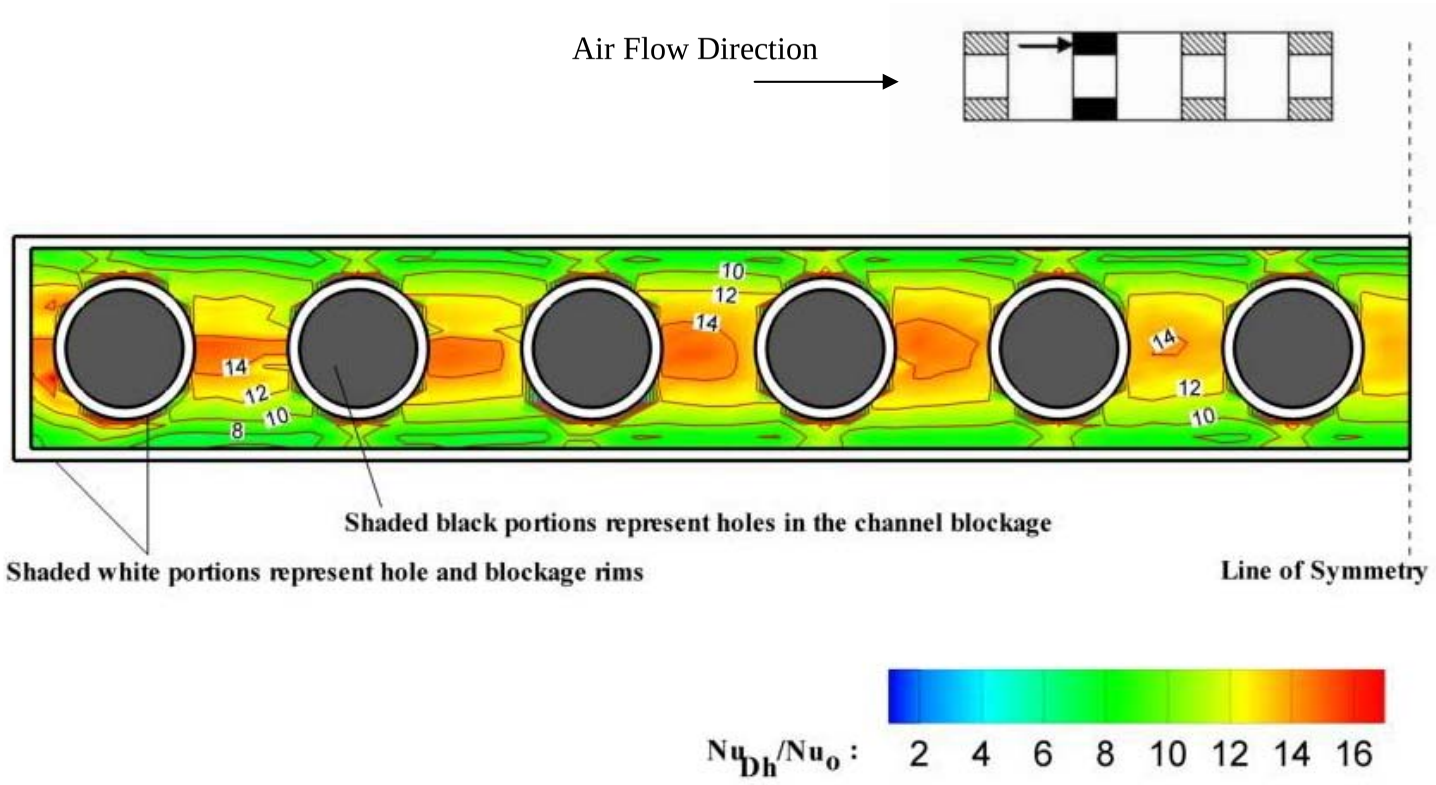

Figure 23: Distribution of Nusselt number ratio, at a Reynolds number of 17,000, on the upstream surface of round holed blockage (case 1) positioned at the second blockage location in the test channel

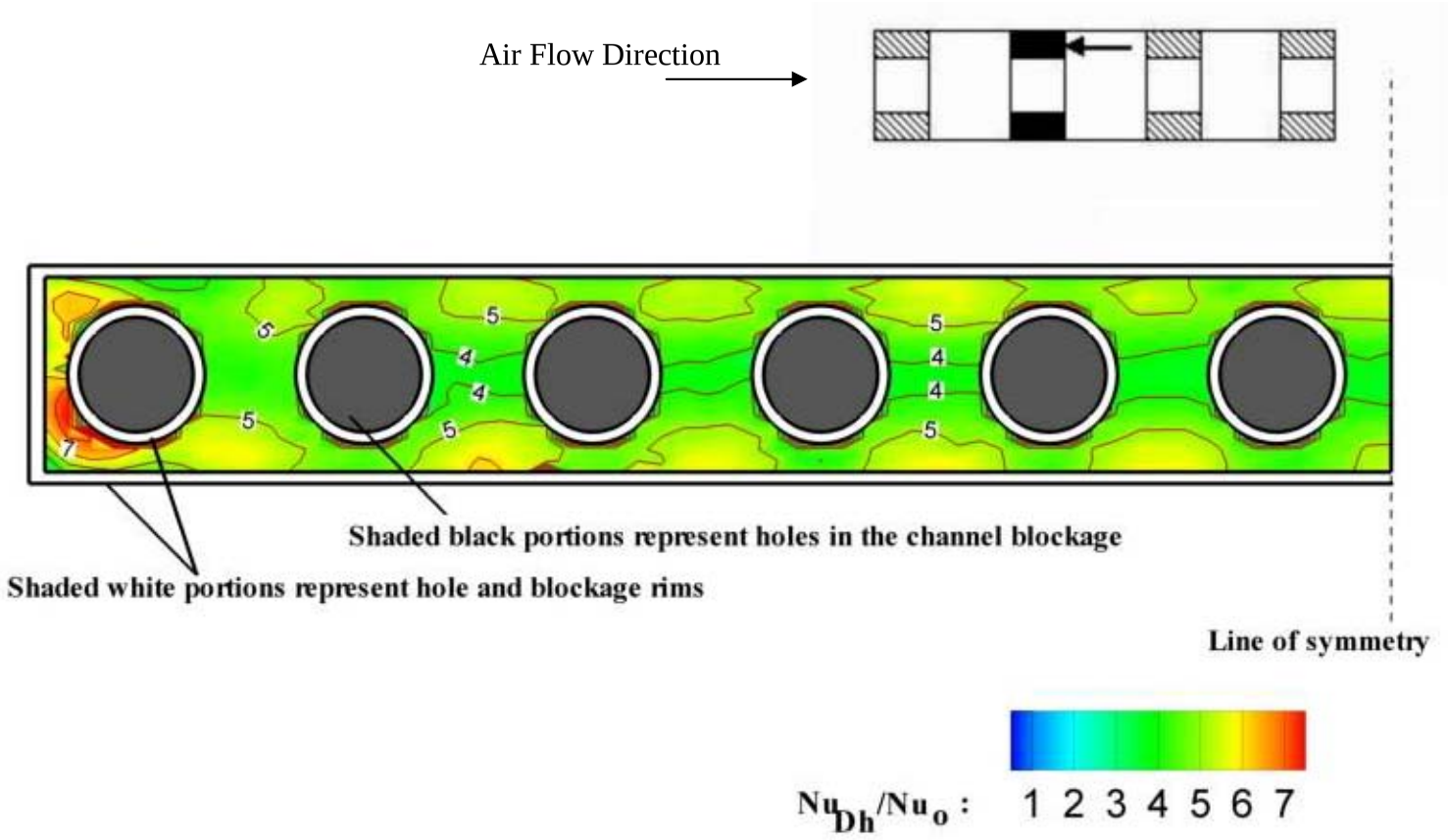

Figure 24: Distribution of local Nusselt number ratio, at a Reynolds number of 17,000, on the downstream surface of round holed blockage positioned at the second blockage location in the test channel

For the case 4 experiments at second blockage location, the maximum value of local Nusselt number ratio on the upstream surface was found to be approximately 12 for low Reynolds number and 10 for high Reynolds number. The downstream surface for both high and low Reynolds number flow consists of a region with Nusselt number ratio comparable to the corresponding maximum Nusselt number ratio on the upstream surface – suggesting air jet reversal from the downstream blockage and re-impingement on the downstream surface of upstream blockage. Nusselt number ratio plots for case 4 experiments at the second blockage location are shown in figures 25-28.

Local Nusselt number ratio is high immediately above and below the blockage holes for on the upstream surface at both low and high Reynolds number indicating a strong secondary flow in these regions.

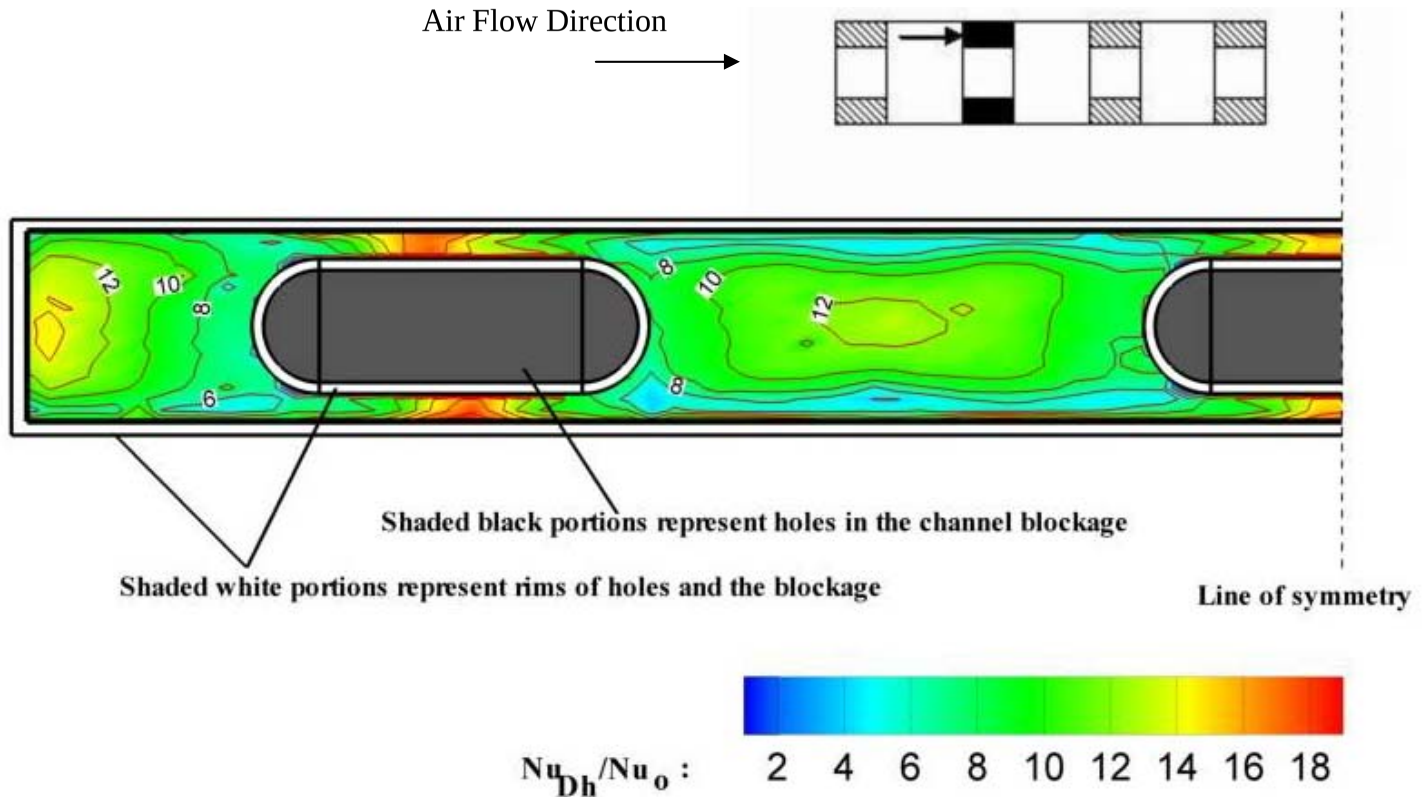

Figure 25: Distribution of Nusselt number ratio, at a Reynolds number of 7,000, on the upstream surface of a case 4 blockage (with most elongated holes) positioned at the second blockage location in the test channel

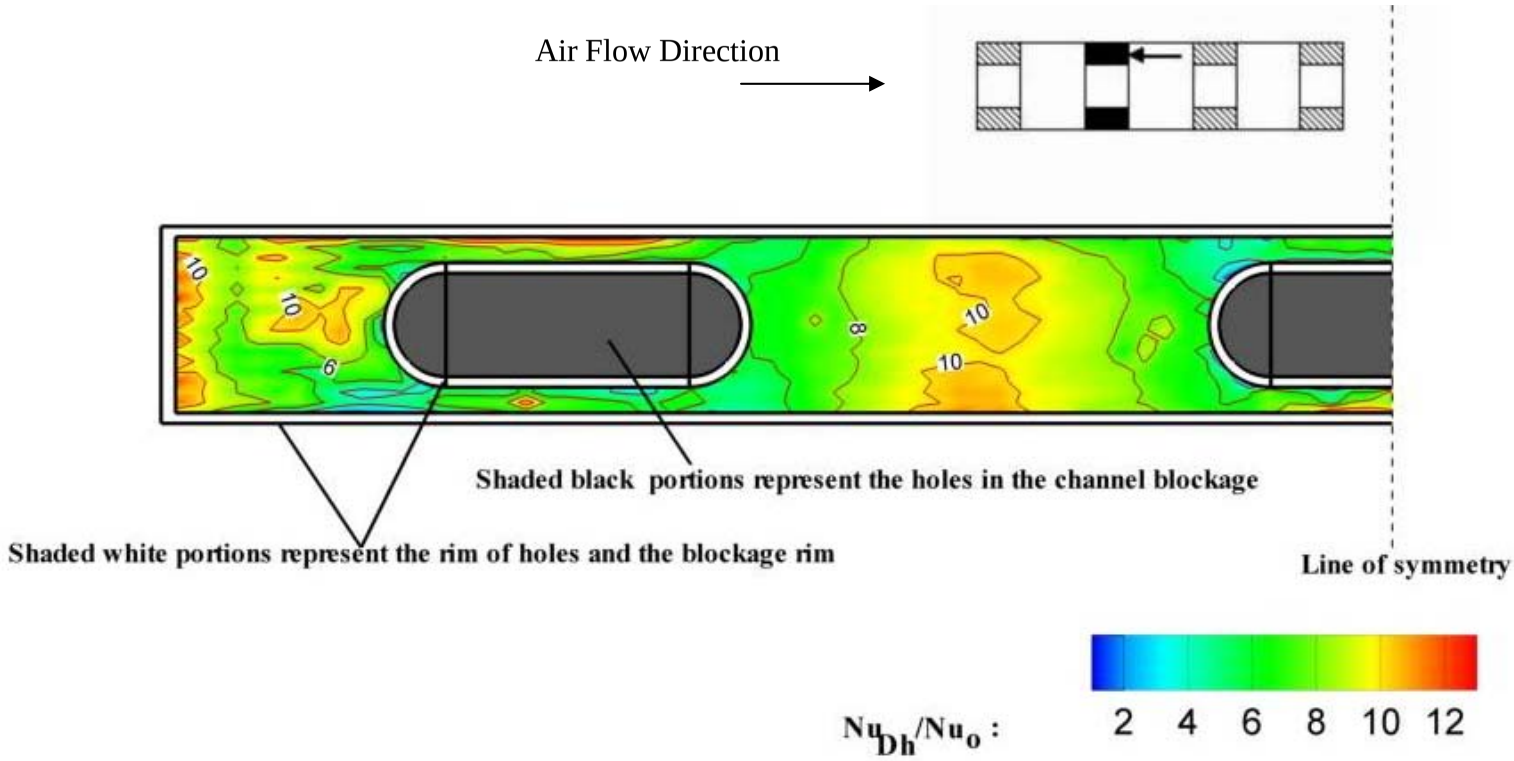

Figure 26: Distribution of Nusselt number ratio, at a Reynolds number of 7,000, on the downstream surface of a case 4 blockage (with most elongated holes) positioned at the second blockage location in the test channel

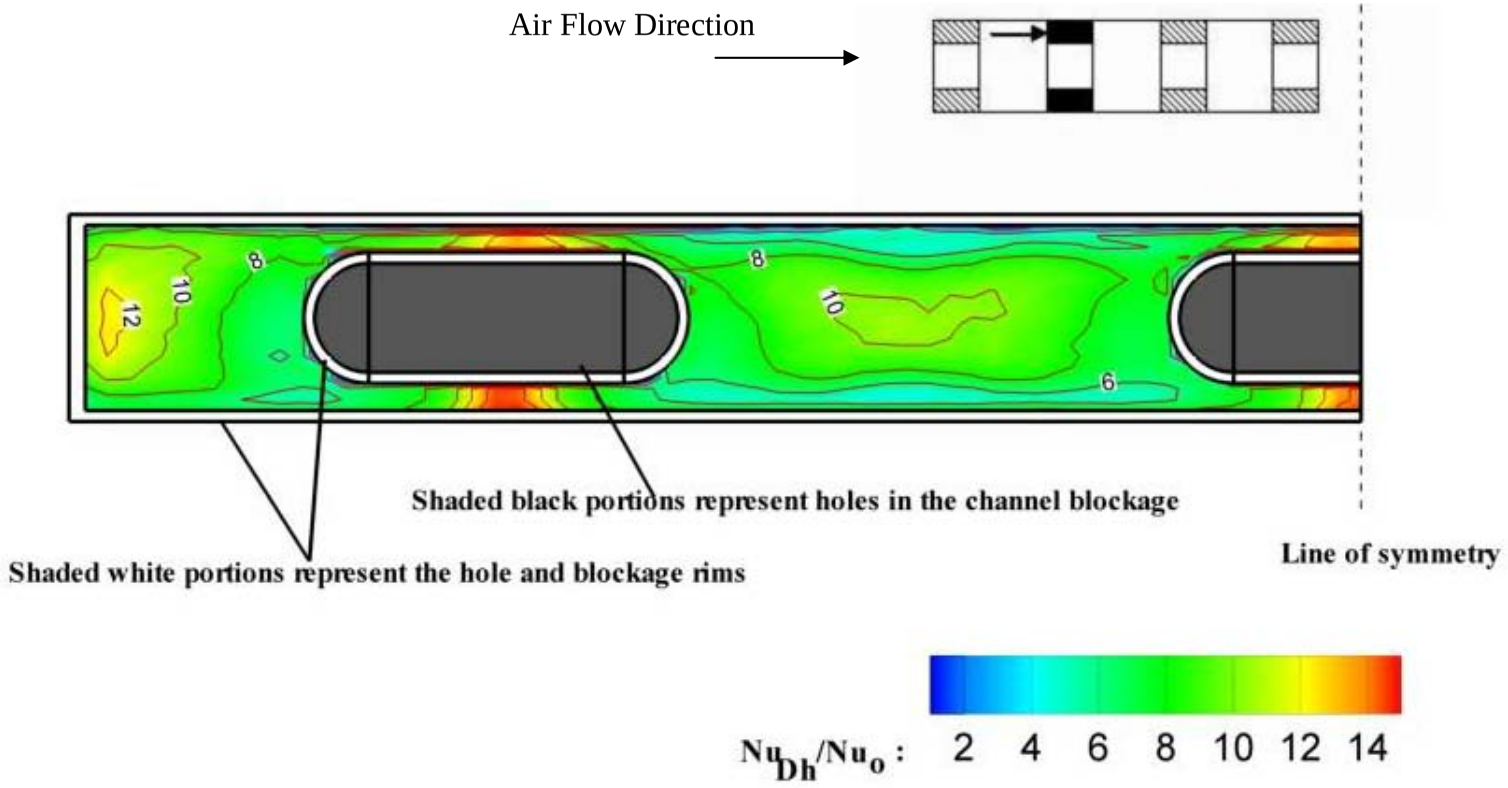

Figure 27: Distribution of Nusselt number ratio, at a Reynolds number of 17,000, on the upstream surface of a case 4 blockage (with most elongated holes) positioned at the second blockage location in the test channel

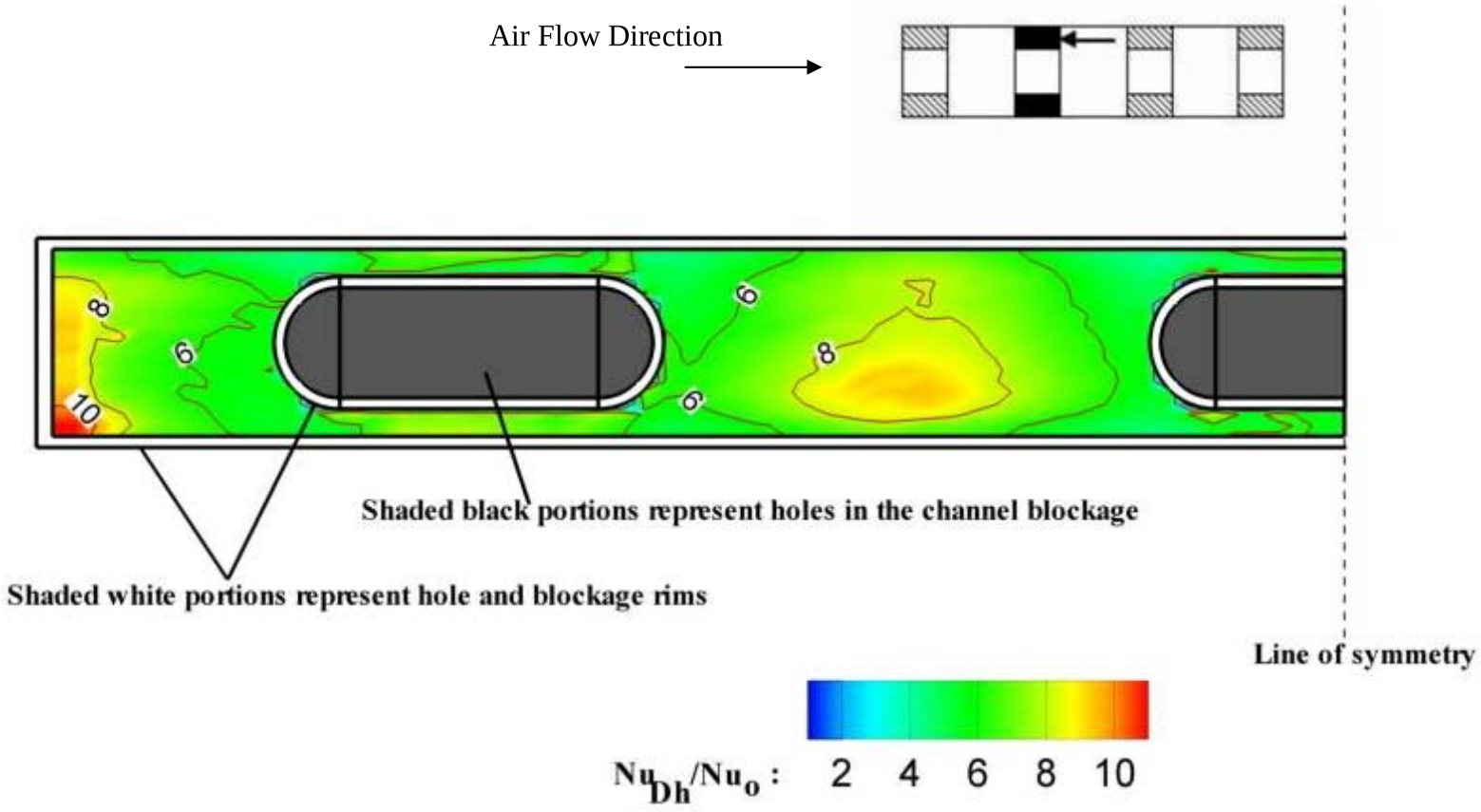

Figure 28: Distribution of Nusselt number ratio, at a Reynolds number of 17,000, on the downstream surface of a case 4 blockage (with most elongated holes) positioned at the second blockage location in the test channel

CHAPTER VIII

CONCLUSIONS AND RECOMMENDATIONS

From the naphthalene sublimation experiments conducted with four different blockage configurations, several conclusions can be drawn. It is to be noted that experiments were conducted at first three blockage locations for two Reynolds numbers – 7,000 and 17,000 based on channel hydraulic diameter. All four cases of blockages result in very high friction factor ratios due to low P/e ratio (rib spacing to rib height ratio) and hole area to channel area ratio.

On the upstream surface at second and third blockage locations, a decrease in heat transfer enhancement was observed with increasing hole elongation. This is due to improved turbulent mixing of air jets between any two blockage locations as the elongation of blockage holes increases. As a result of mixing, the effective velocity of impingement of the air jets on the downstream blockage is low and hence a downward trend is observed in heat transfer enhancement with blockage hole elongation, in spite of the fact that the hole area to channel area ratio is a constant for all blockage configurations.

On the downstream surface at second and third blockage locations, an increase in heat transfer enhancement was observed with increasing hole elongation i.e. configuration 4 blockage had the highest heat transfer enhancement on the downstream surface, while configuration 1 blockages had the least heat transfer enhancement. Primary reason for this is the jet reversal at the downstream blockage and re-impingement of reversed flow on the downstream surface, observed predominantly in most elongated hole blockage case. Jet reversal is minimal with configuration 1 and configuration 2 blockages – hence a very low downstream heat transfer enhancement has been observed.

At the first blockage location the upstream flow behaviour is different from that at the second or third blockage locations. At second and third blockage locations, there is direct impingement of primary air jets on the naphthalene surface of a blockage case unlike at first blockage location, where the impingement is caused by shear established due to primary jet of air being drawn downstream of the channel from the section ahead of first blockage.

If the average values of upstream and downstream Nusselt number ratios are compared for all the blockage configurations tested, at any of the three blockage locations, it can be observed that case 1 blockages result in best heat transfer enhancement. Interestingly, case 4 blockages, though with a lesser value for heat transfer enhancement, are nearly equal in the heat transfer enhancement. A similar observation can be made about the thermal performance characteristics of the four blockage configurations tested.

In summary, the heat transfer enhancement, measured as the Nusselt number ratio, ranged between 3.8 and 12.4 for all blockage configurations and both Reynolds numbers on the upstream surface. The range of heat transfer enhancement on the downstream side was between 3.6 and 7.5. Heat transfer coefficient ranged between 60 and 290 W/m^2K for all blockage cases, Reynolds numbers and blockage locations experimented.

As mentioned in the very start of this section, it can be seen that friction factors are high with all the blockage configurations, particularly so with case 2, case 3 and case 4. New ideas on reducing the pressure drop while maintaining the heat transfer enhancement have to be experimented. Also, in order that a complete channel thermal performance can be estimated, results of channel wall heat transfer studies and those on heat transfer from the blockage surfaces have to be combined to make a holistic comparison of performance of different configurations. It is hoped that the results of this investigation would prove invaluable to heat transfer equipment (in particular, gas turbine) designers.

REFERENCES

[1] Han, J.C., Dutta, S., Ekkad, S.V., 2000, *Gas Turbine Heat Transfer and Cooling Technology*, Taylor and Francis, Buffalo, NY

[2] Mills, A.F., 1999, *Basic Heat and Mass Transfer*, Prentice Hall, Upper Saddle River, NJ 07485

[3] Ambrose, D., Lawrenson, I.J., and Sprake, C.H.S., 1975, The Vapor Pressure of Naphthalene, *Journal of Chemical Thermodynamics*, **7**, pp. 1172-1176

[4] Lau, S.C., 2001, Enhanced internal cooling of gas turbine airfoils, in: B.Sunden, M.Faghri (Eds.), *Heat Transfer in Gas Turbines*, WIT Press, Southampton, UK, pp. 109-173

[5] White, L. and Wilkie, D., 1970, The Heat Transfer and Pressure Loss Characteristics of Some Multi-Start Ribbed Surfaces, *Augmentation of Convection Heat and Mass Transfer* (Edited by Burgles, A.E. and Webb R.L.), ASME, New York, pp.55-62

[6] Gee, D.L. and Webb, R.L.,1970, Forced Convection Heat Transfer in Helically Rib-Roughened Tubes, *International Journal of Heat and Mass Transfer*, **23**, pp.1127-1136

[7] Han, J.C., 1970, Heat Transfer and Friction in Channels with Two Opposite Rib-Roughened Walls, ASME *Journal of Heat Transfer*, **106**, pp.55-62

[8] Han, J.C., Park, J.S., and Lei, C.K.,1985, Heat Transfer Enhancement in Channels with Turbulence Promoters, *ASME Journal of Engineering for Gas Turbines*, **107**, pp.628-635

[9] Han, J.C., and Park, J.S., 1988, Developing Heat Transfer in Rectangular Channels with Rib Turbulators, *International Journal of Heat and Mass Transfer*, **31**, pp. 183-195

[10] Liou, T.M. and Hwang, J.J., 1992, Turbulent Heat Transfer Augmentation and Friction in Periodic Fully Developed Channel Flows, *ASME Journal of Heat Transfer*, **114**, pp.56-64

[11] Lau, S.C., McMillin, R.D., and Han, J.C., 1991, Turbulent Heat Transfer and Friction in a Square Channel with Discrete Turbulators, *ASME Journal of Turbomachinery*, **113**, pp.360-366

[12] Lau, S.C., Kukreja, R.T., and McMillan, R.D., 1991, Effects of V-Shaped Rib Arrays on Turbulent Heat Transfer and Friction of Fully Developed Flow in a Square Channel, *International Journal of Heat and Mass Transfer*, **34**, pp. 1605-1616

[13] Han, J.C., Zhang, Y.M., and Lee, C.P., 1991, Augmented Heat Transfer in Square Channels with Parallel, Crossed and V-Shaped Angled Ribs, *ASME Journal of Heat Transfer*, **113**, pp. 590-596,

[14] Han, J.C., Zhang, Y.M., and Lee, C.P., 1992, Influence of Surface Heat Flux Ratio on Heat Transfer Augmentation in Square Channels with Parallel, Squared and V-Shaped Angled Ribs, *ASME Journal of Turbomachinery*, **114**, pp. 872-880

[15] Olsson, C.-O, and Sunden, B., 1998, Experimental Study of Flow and Heat Transfer in Rib-Roughened Rectangular Channels, *Experimental Thermal and Fluid Science*, **16**, pp.349-365

[16] Taslim, M.E., and Spring, S.D., 1994, Effects of Turbulator Profile and Spacing on Heat Transfer and Friction in a Channel, *AIAA Journal of Thermophysics and Heat Transfer*, **8**, pp. 555-562

[17] Han, J.C., Huang, J.J., and Lee, C.P., 1993, Augmented Heat Transfer in Square Channels with Wedge Shaped and Delta Shaped Turbulence Promoters, *Journal of Enhanced Heat Transfer*, **1**, pp. 37-52

[18] Chyu, M.K., Yu, Y., Ding, H., Downs, J.P., Soechting, F.O., 1997, Concavity Enhanced Heat Transfer in an Internal Cooling Passage, *ASME Paper No. 97-GT-437*

[19] Moon, H.K., O'Connell, T., and Glezer, B., 1999, Channel Height Effect on Heat Transfer and Friction in a Dimpled Passage, *ASME Paper No. 99-GT-163*

[20] Kukreja, R.T., Lau, S.C., and Spence, R.B., 1998, Local Heat Transfer Distributions in a Square Channel with Solid and Perforated Ribs on Two Opposite Walls, *Journal of Enhanced Heat Transfer*, **5**, pp. 9-22

[21] Lau, S.C., Spence, R.B., and Kukreja R.T., 1997, Effects of Ribs with Holes on Heat Transfer in a Square Channel, *AIAA Journal of Thermophysics and Heat Transfer*, **11**, pp. 484-486

[22] Moon, S.W., Lau, S.C., 2003, Heat Transfer between Blockages with Holes in a Rectangular Channel, *ASME Journal of Heat Transfer*, **125**, pp. 587-594

[23] Lau, S.C., Cervantes, J., Han, J.C., Rudolph, R.J., Flannery, K., 2003, Measurement of Wall Heat (Mass) Transfer for Flow through Blockages with Round and Square Holes in a Wide Rectangular Channel, *International Journal of Heat and Mass Transfer*, **46**, pp. 3991-4001

[24] Wagner, J.H., Johnson, B.V., and Graziani, R.A., and Yeh, F.C., 1992, Heat Transfer in Rotating Serpentine Passages with Trips Normal to the Flow, *ASME Journal of Turbomachinery*, **114**, pp.847-857

[25] Johnson, B.V., Wagner, J.H., Steuber, G.D., and Yeh, F.C., 1975, Heat Transfer in Rotating Square Channel With Trips Skewed to the Flow, *ASME Journal of Turbomachinery*, **116**, pp. 113-123.

[26] Kim, H.M., and Kim, K.Y., 2004, Design Optimization of Rib-Roughened Channel to Enhance Turbulent Heat Transfer, *International Journal of Heat and Mass Transfer*, **47**, pp. 5159-5168

[27] Coleman, H.W. and Steele, W.G., 1989, *Experimentation and Uncertainty Analysis for Engineers*, John Wiley and Sons, New York, NY

[28] Lau, S.C., 2001, *Instruction Manual*, Heat Transfer Laboratory, Texas A&M University, College Station, TX-77840.

[29] Goldstein, R.J., and Cho, H.H., 1995, A Review of Mass Transfer Measurements Using Naphthalene Sublimation, *Experimental Thermal and Fluid Sciences*, **10**, pp. 416-434.

[30] Eckert, E.R.G., 1976, Analogies to Heat Transfer Processes, *Measurements in Heat Transfer*, Hemisphere Publishing Corp., New York, NY.

[31] Incropera, F.P., and DeWitt, D.P., 2002, *Fundamentals of Heat and Mass Transfer*, John Wiley & Sons, New York, NY.

[32] Sparrow, E.M., Goldstein R.J., Rouf, M.A.,1975, Effect of Nozzle-Surface Separation Distance on Impingement Heat Transfer for a Jet in a Cross Flow, *Transactions of American Society of Mechanical Engineers*, Series C, *Journal of Heat Transfer*, **97**, pp. 528-533

[33] Goldstein R.J., and Behbahani, A.I., 1982, Impingement of a Circular Jet With and Without Cross Flow, *International Journal of Heat and Mass Transfer*, **25**, No.9, pp. 1377-1382

[34] Mills, A.F., 1992, *Heat Transfer*, Prentice Hall, Upper Saddle River, NJ 07485

APPENDIX A

EXPERIMENTAL RESULTS

Experimental results

For the ease of discussion and presentation of results, a naming convention has been adopted to identify each experimental case. Each case is identified with a number indicating the blockage configuration, an alphabet (a, b, or c) suggesting the aluminium blockage (of same configuration as the other three similar configuration acrylic blockages positioned in the channel) location in the channel, another number to identify if the experiment has been performed at low (1) or high (2) Reynolds number, and 'Up' or 'Dn' to identify if the upstream or downstream surface of the blockage is being studied for heat transfer characteristics. For example, '1a1Up' would represent an experiment with first (1) blockage configuration, the aluminium blockage with this configuration positioned at first location (a), low (1) Reynolds number experiment to determine the heat transfer distribution on the upstream (Up) face of the aluminium blockage. Similarly, '4b2Dn' would represent a high (2) Reynolds number experiment with fourth (4) blockage configuration, to study the heat transfer characteristics on the downstream (Dn) surface of the aluminium blockage of this configuration positioned at second (b) location. This notation has been primarily used to list results for each experiment in this appendix section.

Table 1: Experimental results for case 1 and case 2 blockages at first blockage location

Case	1a1Up	1a1Dn	1a2Up	1a2Dn	2a1Up	2a1Dn	2a2Up	2a2Dn
Δt (s)	2700	2700	1500	1500	2700	2700	1500	1500
P_0 (Pa)	100831	100824	98371	98418	100712	100714	97802	97871
ΔP (Pa)	333.0	336.3	2084.1	2059.1	338.8	340.0	2046.7	2100.7
T_o(K)	299.6	299.6	298.5	299.1	298.9	299.0	298.9	298.8
T (K)	299.6	299.5	298.3	298.9	298.8	298.9	298.8	298.8
mass flow rate of air (Kg/s)	0.0211	0.0212	0.0513	0.0510	0.0213	0.0213	0.0507	0.0513
Re_{Dh}	6938	6972	16894	16764	7012	7020	16674	16898
Nu_o	23.7	23.8	48.4	48.1	23.9	23.9	47.8	48.4
Sh_o	37.8	38.0	77.1	76.6	38.2	38.2	76.3	77.1
P_{vw} (Pa)	12.91	12.74	11.43	12.10	11.98	12.08	11.92	11.95
$\rho_{vw} * 10^4$ (Kg/m^3)	6.64	6.56	5.90	6.24	6.18	6.23	6.15	6.16
h_m (m/s)	0.036	0.025	0.059	0.042	0.029	0.026	0.045	0.044
Sh_{Dh}	238.90	168.23	398.79	281.93	193.99	178.01	300.97	295.22
Nu_{Dh}	149.81	105.49	250.07	176.80	121.65	111.63	188.74	185.13
Nu_{Dh}/Nu_o	6.31	4.43	5.17	3.68	5.08	4.66	3.94	3.83
h(W/m^2K)	83.60	58.86	139.12	98.50	67.74	62.19	105.10	103.06
Friction factor ratio - blockage 1	878.43	871.53	1042.03	1036.23	1111.40	1135.34	1297.43	1302.99
Friction factor ratio - blockage 2	752.94	747.03	1053.16	940.17	978.21	965.95	1078.43	986.84
Friction factor ratio - blockage 3	641.40	650.19	767.59	862.50	762.36	764.52	1171.40	1065.63
Thermal Performance	0.66	0.46	0.51	0.36	0.49	0.45	0.36	0.35

Table 2: Experimental results for case 3 and case 4 blockages at first blockage location

Case	3a1Up	3a1Dn	3a2Up	3a2Dn	4a1Up	4a1Dn	4a2Up	4a2Dn
Δt (s)	2940	2700	1500	1563	2700	2700	1500	1500
P_0 (Pa)	100604	100589	97270	97317	100501	100510	96992	97079
ΔP (Pa)	337.9	341.7	2030.1	2021.8	336.3	335.9	1835.0	1851.6
T_o(K)	300.1	299.9	298.3	300.7	297.8	298.3	298.9	299.0
T (K)	300.2	299.7	298.3	300.8	297.9	298.3	298.7	298.8
mass flow rate of air (Kg/s)	0.0212	0.0214	0.0504	0.0501	0.0212	0.0212	0.0478	0.0481
Re_{Dh}	6967	7008	16605	16413	7012	6993	15744	15813
Nu_o	23.8	23.9	47.7	47.2	23.9	23.9	45.7	45.9
Sh_o	38.0	38.1	76.1	75.3	38.2	38.1	72.9	73.1
P_{vw} (Pa)	13.67	13.03	11.37	14.55	10.94	11.41	11.80	11.96
$\rho_{vw} * 10^4$ (Kg/m^3)	7.02	6.70	5.87	7.45	5.66	5.89	6.09	6.17
h_m (m/s)	0.027	0.033	0.043	0.052	0.028	0.037	0.042	0.056
Sh_{Dh}	182.21	221.42	287.50	347.72	188.96	248.33	284.85	377.19
Nu_{Dh}	114.26	138.85	180.29	218.05	118.50	155.72	178.63	236.53
Nu_{Dh}/Nu_o	4.80	5.81	3.78	4.62	4.95	6.52	3.91	5.16
h (W/m^2K)	63.85	77.54	100.21	122.05	65.77	86.57	99.47	131.76
Friction factor ratio - blockage 1	1121.85	1162.53	1270.63	1259.39	1140.28	1108.02	1283.89	1122.43
Friction factor ratio - blockage 2	1135.65	1139.74	1447.37	1430.94	1274.70	1256.38	1670.77	1576.15
Friction factor ratio - blockage 3	1112.66	1103.26	1419.13	1427.80	1372.04	1419.10	1736.96	1775.29
Thermal Performance	0.46	0.55	0.35	0.43	0.47	0.63	0.36	0.50

Table 3: Experimental results for case 1 and case 2 blockages at second blockage location

Case	1b1Up	1b1Dn	1b2Up	1b2Dn	2b1Up	2b1Dn	2b2Up	2b2Dn
Δt (s)	2700	2700	1500	1500	2700	2700	1500	1500
P_0 (Pa)	100816	100822	98392	98384	100765	100751	98028	98008
ΔP (Pa)	337.5	336.7	2046.7	2046.7	338.3	335.9	2046.7	2046.7
T_o(K)	298.0	297.9	299.0	298.7	299.5	300.0	299.5	299.7
T (K)	297.8	297.9	298.9	298.6	299.6	299.8	299.4	299.7
mass flow rate of air (Kg/s)	0.0213	0.0213	0.0508	0.0508	0.0213	0.0212	0.0507	0.0507
Re_{Dh}	7029	7022	16718	16740	6991	6953	16653	16636
Nu_o	24.0	24.0	48.0	48.0	23.9	23.8	47.8	47.8
Sh_o	38.2	38.2	76.5	76.5	38.1	37.9	76.2	76.2
P_{vw} (Pa)	10.84	10.93	12.07	11.75	12.87	13.22	12.71	13.02
$\rho_{vw} * 10^4$ (Kg/m^3)	5.61	5.65	6.22	6.06	6.62	6.79	6.54	6.70
h_m (m/s)	0.067	0.027	0.119	0.054	0.064	0.029	0.110	0.058
Sh_{Dh}	450.27	181.65	803.14	363.91	426.81	195.58	736.54	385.96
Nu_{Dh}	282.36	113.91	503.64	228.21	267.65	122.65	461.88	242.03
Nu_{Dh}/Nu_o	11.78	4.76	10.50	4.75	11.21	5.16	9.66	5.07
h(W/m^2K)	156.82	63.26	280.52	126.99	149.32	68.52	257.63	135.09
Friction factor ratio - blockage 1	940.12	918.92	1090.19	1088.62	1111.00	1121.61	1191.93	1189.78
Friction factor ratio - blockage 2	741.95	743.44	944.28	904.61	803.41	987.76	1209.45	1236.13
Friction factor ratio - blockage 3	668.22	664.94	873.38	903.58	661.09	673.89	879.79	895.17
Thermal Performance	1.20	0.49	1.02	0.46	1.08	0.50	0.91	0.48

Table 4: Experimental results for case 3 and case 4 blockages at second blockage location

Case	3b1Up	3b1Dn	3b2Up	3b2Dn	4b1Up	4b1Dn	4b2Up	4b2Dn
Δt (s)	2700	2700	1500	1500	2700	2700	1200	1500
P_0 (Pa)	100581	100569	97104	97098	100461	100471	96501	96493
ΔP (Pa)	337.1	338.3	2055.0	2055.0	337.1	335.9	2001.0	2017.6
T_o(K)	299.4	300.1	300.4	299.9	298.5	299.3	299.9	301.1
T (K)	299.2	300.2	300.4	299.8	298.2	299.1	300.1	301.4
mass flow rate of air (Kg/s)	0.0212	0.0212	0.0505	0.0505	0.0212	0.0212	0.0497	0.0498
Re_{Dh}	6977	6967	16544	16576	7000	6964	16313	16297
Nu_o	23.8	23.8	47.5	47.6	23.9	23.8	47.0	47.0
Sh_o	38.0	38.0	75.8	75.9	38.1	37.9	75.0	74.9
P_{vw} (Pa)	12.49	13.64	14.02	13.16	11.31	12.31	13.57	15.37
$\rho_{vw} * 10^4$ (Kg/m^3)	6.43	7.00	7.19	6.76	5.85	6.34	6.97	7.86
h_m (m/s)	0.060	0.038	0.097	0.067	0.053	0.043	0.097	0.071
Sh_{Dh}	403.51	254.04	646.77	447.18	360.79	285.61	650.03	471.41
Nu_{Dh}	253.04	159.30	405.58	280.42	226.25	179.10	407.62	295.62
Nu_{Dh}/Nu_o	10.62	6.69	8.53	5.89	9.47	7.53	8.67	6.29
h(W/m^2K)	141.12	89.03	226.83	156.62	125.83	99.85	227.67	165.68
Friction factor ratio - blockage 1	1157.66	1120.95	1288.40	1295.39	1202.00	1217.90	1364.91	1359.94
Friction factor ratio - blockage 2	1231.45	1267.96	1548.98	1535.43	1294.46	1333.67	1615.97	1536.14
Friction factor ratio - blockage 3	1042.35	1056.63	1338.03	1358.50	1465.52	1329.04	1989.38	1994.02
Thermal Performance	1.01	0.64	0.78	0.54	0.89	0.70	0.78	0.57

Table 5: Experimental results for case 1 and case 4 blockages at third blockage location (Only low Re experiments conducted).

Case	1c1Up	1c1Dn	4c1Up	4c1Dn
Δt (s)	2700	2700	2700	2700
P_0 (Pa)	100826	100824	100522	100530
ΔP (Pa)	336.7	336.3	336.3	336.3
T_o(K)	298.8	299.0	299.3	300.0
T (K)	298.6	298.8	298.9	299.7
mass flow rate of air (Kg/s)	0.0213	0.0212	0.0212	0.0212
Re_{Dh}	6998	6988	6969	6950
Nu_o	23.9	23.9	23.8	23.8
Sh_o	38.1	38.1	38.0	37.9
P_{vw} (Pa)	11.78	11.92	12.09	13.11
$\rho_{vw} * 10^4$ (Kg/m^3)	6.08	6.15	6.23	6.74
h_m (m/s)	0.070	0.028	0.061	0.038
Sh_{Dh}	471.27	185.85	411.66	253.92
Nu_{Dh}	295.53	116.54	258.15	159.23
Nu_{Dh}/Nu_o	12.37	4.88	10.84	6.70
h(W/m^2K)	164.53	64.91	143.93	88.95
Friction factor ratio - blockage 1	931.56	955.34	1183.80	1177.94
Friction factor ratio - blockage 2	779.37	747.66	1359.52	1362.71
Friction factor ratio - blockage 3	558.01	632.28	998.83	946.97
Thermal Performance	1.27	0.50	1.02	0.63

APPENDIX B

UNCERTAINTY ANALYSIS

Measured variables for the mass transfer experiments are P_o (Upstream pressure at the orifice), ΔPo (pressure drop across the orifice), T_o (temperature upstream of the orifice), T_w (wall temperature), ΔM_n (effective mass of naphthalene convection during experiment), Δt (effective duration of experiment), Δp (pressure drop across any blockage).

Resolution of manometer used is 0.01 inches of water. Bias values for estimating uncertainties in P_o, ΔPo are taken as half the resolution of the manometer used. Three readings for P_o and ΔPo are taken during the experiment. Using this data, uncertainty in P_o and ΔPo are calculated. Thermocouple measurements of T_o and T_w during an experiment are used to estimate the uncertainty in the corresponding temperatures. Since the thermocouples were calibrated before experimentation, bias is eliminated in the temperature measurements. Uncertainty in mass measurements (ΔM_n) is taken as 1mg and uncertainty in time duration measurement (Δt) is taken as 5 seconds. Uncertainty in Δp is calculated using the pressure transducer voltage measurements taken during the experiment. Uncertainty in properties of air is taken as 1% of the property value and uncertainty in diffusion coefficient (σ) is taken as 5%. Other uncertainty estimates are discussed below.

Mass flow rate of air: $\dot{m} = 0.25\pi d_o^2 CY(2P_o\Delta P_o)/RT_o(1-\eta^4)$

$$\frac{U_{\dot{m}}}{\dot{m}} = \sqrt{(\frac{U_{P_o}}{2P_o})^2 + (\frac{U_{\Delta P}}{2\Delta P})^2 + (\frac{U_{To}}{2T_o})^2}$$

Maximum uncertainty in $\dot{m}$ was found to be approximately ±2.8%.

Reynolds number: $\mathrm{Re}_{Dh} = \rho \overline{V} D_h / \mu = 4\dot{m} / \mu P$

$$\frac{U_{\mathrm{Re}_{Dh}}}{\mathrm{Re}_{Dh}} = \sqrt{(\frac{U_{\dot{m}}}{\dot{m}})^2 + (\frac{U_{\mu}}{\mu})^2 + (\frac{U_p}{P})^2}$$

Maximum uncertainty in Reynolds number was found to be approximately ±3%.

Overall mass transfer coefficient: $\bar{h}_m = (\Delta M_n / \rho_{v,w} A_s \Delta t)$

$$\frac{U_{\bar{h}_m}}{\bar{h}_m} = \sqrt{(\frac{U_{\Delta M_n}}{\Delta M_n})^2 + (\frac{U_{\Delta t}}{\Delta t})^2 + (\frac{U_{A_s}}{A_s})^2 + (\frac{U_{\rho_{v,w}}}{\rho_{v,w}})^2}$$

Maximum uncertainty value for $\bar{h}_m$ was found to be ±13.8%.

Local mass transfer coefficient: $h_m = \dfrac{(\rho_s \Delta z / \Delta t)}{\rho_{v,w}}$

$$\frac{U_{h_m}}{h_m} = \sqrt{(\frac{U_{\rho_s}}{\rho_s})^2 + (\frac{U_{\Delta z}}{\Delta z})^2 + (\frac{U_{\Delta t}}{\Delta t})^2 + (\frac{U_{\rho_{v,w}}}{\rho_{v,w}})^2}$$

Uncertainty in the value of local mass transfer coefficient is about ±6.3%.

Overall Sherwood number: $\overline{Sh}_{Dh} = \bar{h}_m D_h / \sigma$

$$\frac{U_{\overline{Sh}_{Dh}}}{\overline{Sh}_{Dh}} = \sqrt{(\frac{U_{\bar{h}_m}}{\bar{h}_m})^2 + (\frac{U_{A_c}}{A_c})^2 + (\frac{U_p}{P})^2 + (\frac{U_\sigma}{\sigma})^2}$$

Maximum uncertainty in $\overline{Sh}_{Dh}$ is about ±7.2%.

Friction factor: $f = 2\rho \Delta p (A_c / \dot{m})^2$

$$\frac{U_f}{f} = \sqrt{(\frac{U_\rho}{\rho})^2 + (\frac{U_{\Delta p}}{\Delta p})^2 + (\frac{2U_{A_c}}{A_c})^2 + (2\frac{U_{\dot{m}}}{\dot{m}})^2}$$

Maximum uncertainty in friction factor was determined as approximately ±8.3%.

VITA

Name: Praveen Venkata Panduranga Rupakula

Address: 419A ENPH, Texas A&M University, Department of Mechanical Engineering, 3123 TAMU, College Station, TX 77843-3123

Email Address: praveenrvp at tamu dot edu

Phone: (979) 845-1836

Education: B.S., Mechanical Engineering, 2003
Jawaharlal Nehru Technological University (JNTU), India
M.S., Mechanical Engineering, 2005
Texas A&M University, College Station, USA.